การเปรียบเทียบการเร่งอนุภาคที่บริเวณอัดอย่างต่อเนื่องและที่คลื่นกระแทก

นางสาวกมลพร กลับพงศ์

วิทยานิพนธ์นี้เป็นส่วนหนึ่งของการศึกษาตามหลักสูตรปริญญาวิทยาศาสตรมหาบัณฑิต
สาขาวิชาฟิสิกส์ ภาควิชาฟิสิกส์
คณะวิทยาศาสตร์ จุฬาลงกรณ์มหาวิทยาลัย
ปีการศึกษา 2544
ISBN 974-17-0281-7

COMPARISON BETWEEN PARTICLE ACCELERATION AT A CONTINUOUS COMPRESSION AND AT A SHOCK

Miss Kamonporn Klappong

A Thesis Submitted in Partial Fulfillment of the Requirements
for the Degree of Master of Science in Physics
Department of Physics
Faculty of Science
Chulalongkorn University
Academic Year 2001
ISBN 974-17-0281-7

Thesis Title	Comparison between Acceleration at a Continuous Compression and at a Shock
By	Miss Kamonporn Klappong
Field of Study	Physics
Thesis Advisor	Associate Professor David Ruffolo, Ph.D.

Accepted by the Faculty of Science, Chulalongkorn University in Partial Fulfillment of the Requirements for the Master's Degree

……..…….... Deputy Dean for Administrative Affairs
(Associate Professor Pipat Karntiang, Ph. D.) Acting Dean, Faculty of Science

THESIS COMMITTEE

……Chairman
(Associate Professor Anantasin Techagumpuch, Ph.D.)

……Thesis Advisor
(Associate Professor David Ruffolo, Ph.D.)

……Member
(Ahpisit Ungkitchanukit, Ph.D.)

……Member
(Rattachat Mongkolnavin, Ph.D.)

นางสาวกมลพร กลับพงศ์: การเปรียบเทียบการเร่งอนุภาคที่บริเวณอัดอย่างต่อเนื่องและที่คลื่นกระแทก
(COMPARISON BETWEEN PARTICLE ACCELERATION AT A CONTINUOUS COMPRESSION AND AT A SHOCK)
อ. ที่ปรึกษา : รศ. ดร. เดวิด รูฟโฟโล, 117 หน้า. ISBN 974-17-0281-7.

อนุภาคมีประจุในพลาสมาดาราศาสตร์ สามารถถูกเร่งให้เป็นอนุภาคพลังสูง (รังสีคอสมิก) ตามกลไกการเร่งแบบเฟอร์มีอันดับที่หนึ่ง (the first-order Fermi acceleration) นอกเหนือไปจากบริเวณคลื่นกระแทก บริเวณอัดอย่างต่อเนื่องเป็นอีกแห่งหนึ่งที่กลไกนี้สามารถเร่งอนุภาคได้ เราทำการจำลองการขนส่งอนุภาคในบริเวณใกล้ๆ คลื่นกระแทกหรือบริเวณอัดอย่างต่อเนื่องโดยใช้สมการโฟคเคอร์-แพลงค์ (Fokker-Planck equation) และเลือกสนามแม่เหล็กแบบเฉียง ในการศึกษาเชิงตัวเลขนี้ เราแก้สมการการขนส่งอนุภาคโดยวิธีไฟไนต์ดิฟเฟอร์เรนท์ (finite difference method) การอินเทอร์โพเลต (interpolation) วิธีทีวีดี (TVD method) และเทคนิคการแบ่งแยกตามตัวกระทำการ (operator splitting technique) จากการจำลองเราพบว่าจะมียอดแหลมในกราฟระหว่างความเข้มกับระยะทาง ณ ศูนย์กลางของการอัดที่แคบ ซึ่งความกว้างของการอัดหารด้วยระยะทางอิสระเฉลี่ย ($b/\lambda_{\|}$) มีค่าน้อย ยอดแหลมนี้ไม่พบในแบบจำลองที่ไม่พิจารณากระบวนการเปลี่ยนมุมขั้ว ดังนั้นเราสรุปได้ว่าลักษณะเด่นนี้มีความเกี่ยวพันกับสนามแม่เหล็กที่ทำให้เกิดการสะท้อนกลับของอนุภาค (magnetic mirroring) ณ บริเวณคลื่นกระแทกหรือบริเวณอัดอย่างต่อเนื่อง เราเรียกลักษณะเด่นนี้ว่า “มิเรอริ่ง พี้ค (mirroring peak)” สิ่งที่เกิดขึ้นพร้อมกับ มิเรอริ่ง พี้ค คือความแรงของสเปกตรัมของอนุภาคในสถานะคงตัว (steady-state) โดยเปรียบเทียบกับการประมาณการฟุ้ง (diffusion approximation) ซึ่งไม่รวมการกระจายตัวในมุมขั้ว (pitch angle distribution) ค่าความแรงนี้บ่งชี้ว่า การเร่งจะมีประสิทธิภาพมากสำหรับบริเวณคลื่นกระแทกหรือบริเวณอัดอย่างต่อเนื่องแบบเฉียง เมื่อพลังงานต่ำและค่า $b/\lambda_{\|}$ น้อย เนื่องจากผลของการสะท้อนกลับของอนุภาค

ภาควิชา ฟิสิกส์ ลายมือชื่อนิสิต.....

สาขาวิชา ฟิสิกส์

ปีการศึกษา 2544 ลายมือชื่ออาจารย์ที่ปรึกษา.....

4272204923: MAJOR PHYSICS
KEY WORDS: COSMIC RAYS / ACCELERATION / SHOCK / COMPRESSION / MAGNETIC FIELD
KAMONPORN KLAPPONG: COMPARISON BETWEEN ACCELERATION AT A CONTINUOUS COMPRESSION AND AT A SHOCK. THESIS ADVISOR: ASSOC. PROF. DAVID RUFFOLO, Ph.D. 117 pp. ISBN 974-17-0281-7.

The charged particles in an astrophysical plasma can be accelerated to become energetic particles (cosmic rays) by the first-order Fermi acceleration mechanism. In addition to a shock, a continuous compression is another site where this mechanism can accelerate the particles. We simulate the particle transport near a shock or compression by using a Fokker-Planck equation and choosing an oblique magnetic field. To study this numerically, we solve the equation of particle transport by the finite difference method, interpolation, a TVD method, and the operator splitting technique. From the simulations, we found that there is a peak in intensity vs. distance profiles at the center of a narrow compression region, where the compression width divided by the scattering mean free path ($b/\lambda_{||}$) is small. Such a peak is not found in models that neglect pitch angle processes. Therefore, we conclude that this feature is associated with magnetic mirroring at an oblique shock or compression, and we call this the “mirroring peak.” In association with the mirroring peak, a harder particle spectrum is found in the steady-state (in comparison with the standard diffusion approximation that neglects the pitch angle distribution). This indicates more efficient acceleration for an oblique shock or compression at low energy and low $b/\lambda_{||}$ values, because of magnetic mirroring.

Department of Physics Student’s signature……
Field of study: Physics
Academic year 2001 Advisor’s signature……

Acknowledgments

I would like to extend my sincere gratitude to my advisor, Assoc. Prof. Dr. David Ruffolo, to whom I am indebted. He suggested this topic, and gave guidance and assistance when this work encountered problems.

I would like to express my gratitude to the thesis committee, Assoc. Prof. Dr. Anantasin Techagumpuch, Dr. Ahpisit Ungkitchanukit, and Dr. Rattachat Mongkolnavin for their reading and criticizing the manuscript.

I would like to thank so many people in the computational astrophysics research lab for their kindness and help, especially Miss Piyanate Chuychai and Miss Kanokporn Leerungnavarat for their programs, Mr. Kittipat Malakit for his discussion, Miss Thiranee Khumlumlert and Miss Phantip Hosesomephan for their help.

Finally, I would like to thank my family and Mr. Natthapon Nakpathomkun for their encouragements.

Contents

Contents (cont.)

Contents (cont.)

List of Figures

List of Figures (cont.)

List of Figures (cont.)

List of Figures (cont.)

List of Figures (cont.)

List of Figures (cont.)

List of Tables

Chapter 1
Introduction

1.1 Introduction

In our solar system, interplanetary space contains many types of particles at all energies. The particles have several different origins. Some of them are from remnants of supernove, some come from other galaxies, and other components are released from the Sun in the form of the solar wind, which continuously streams in the radial direction from the Sun and is mostly composed of protons and electrons. Solar flares and coronal mass ejections (CMEs), huge explosions which occur occasionally, rapidly eject the bulk plasma at high speeds from atmosphere of the Sun. If this plasma fluid encounters the interplanetary medium with a velocity difference greater than the sound speed in this fluid, the collision leads to a surface of discontinuity in physical properties such as the magnetic field, plasma speed, plasma density, etc. This discontinuity is called an interplanetary shock. Shocks also occur in other regions of the solar system.

In this work we are interested in compression regions, which are structures related to shocks. A compression region is like a shock, except that the changes in physical quantities take place over a finite, measurable width (see Figures 1.1 and 1.2). The events of shocks and compressions may occur together as shown in Figure 1.1.

Both shocks and compressions are able to accelerate particles to high energies. The particle acceleration at a shock has been studied previously in great

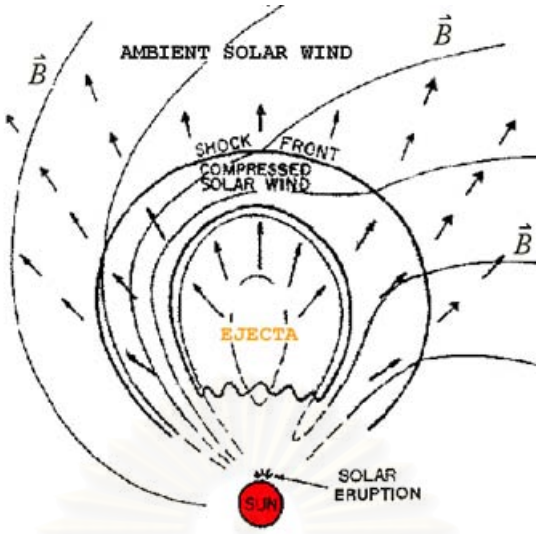

Figure 1.1: This figure shows an eruption on the Sun associated with a CME. The ejecta then travel through interplanetary space. The arrows indicate the direction of the solar wind. The magnetic field lines in the ambient solar wind have a spiral shape, and they are compressed by the faster ejecta. The shock front is a discontinuity in the magnetic field and the fluid flow.

detail (Krymskii 1976; Bell 1978; Ruffolo 1999). Here we are interested in the acceleration at a compression which has a structure like the shock. The acceleration in the compression region is a form of the first-order Fermi acceleration, which is the mechanism believed to account for most of the cosmic ray particle acceleration in the universe. The importance of this mechanism is confirmed by its successful prediction of the power law distribution in momentum of galactic cosmic ray particles measured on the Earth (Fermi 1954). The transport equation that is used to describe the particle acceleration at the continuous compression, assuming hyperbolic magnetic field lines (Ruffolo and Chuychai 1999), is developed from the Fokker-Planck equation (Skilling 1971, 1975). This makes it possible to consider the acceleration of cosmic rays in such regions in detail for the first time in the present work.

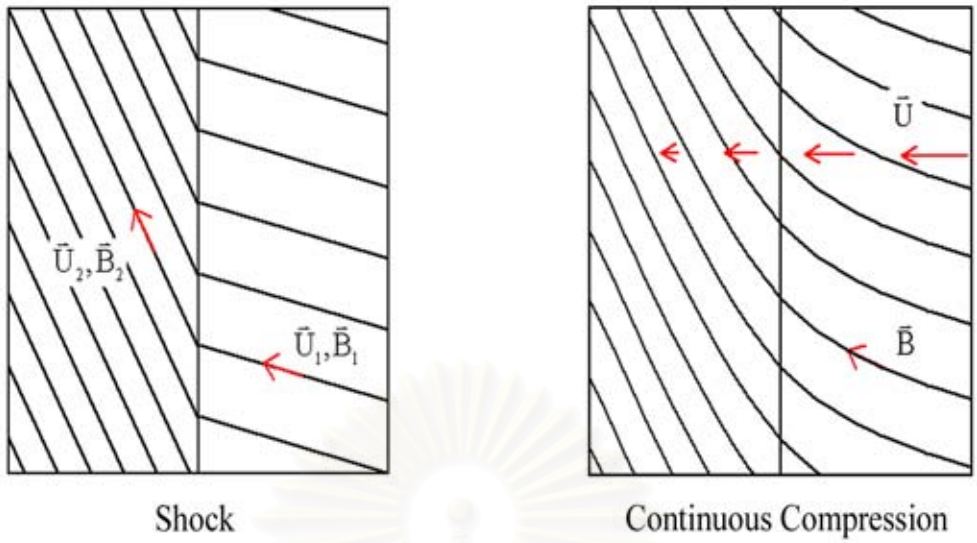

Figure 1.2: Model magnetic field configuration in the shock case and continuous compression case, respectively.

1.2 Objectives

• To develop and test a computer program for the simulation of cosmic ray transport at a fluid compression.

• Study the steady state distribution function of cosmic ray particles near the compression.

• Study the spectral index of particles that are accelerated at the continuous compression region.

• Compare the results from cosmic ray transport simulations for continuous compression region and a shock.

1.3 Outline of this Thesis

The details of the following chapters are as follow. Chapter 2 is about cosmic rays, activity on the Sun, the transport of energetic particles along mag-

netic field lines and the concept of Fermi acceleration. Chapter 3 describes a new equation of cosmic ray transport and explains the configuration of the magnetic field that we use for simulations. The end of this chapter is about the diffusion-convection approximation, which is another way to describe the transport of the cosmic ray particles. The following chapter describes the numerical simulations, which adapt existing numerical techniques to solve our transport equation. We also consider the boundary conditions and the simulation procedure. In Chapter 5 we show results from the simulations including the distribution function, the spectral index, the anisotropy, and the decrease of the distribution function upstream, and discuss the results. The last chapter presents our conclusions.

Chapter 2
Background Knowledge

2.1 Cosmic Rays

Cosmic rays are high energy particles that travel through space to the Earth. The interest in cosmic rays lies in the puzzle of their origin and the mechanisms of how the particles are accelerated to high energy. The data from observations by spacecraft and detectors on the Earth show that the cosmic rays come from all directions over the energy range between 0.1 eV and 3×10^{20} eV. At high energy, there are two specific types of cosmic rays. One type is galactic cosmic rays (GCR), which have an energy between about 10^9 eV and $10^{18.5}$ eV. Another is extragalactic cosmic rays, which have an energy over $10^{18.5}$ eV. Less energetic cosmic rays can frequently be detected in association with activity at the Sun, such as solar flares or CMEs. These are examples of events/sites in the solar system where there are mechanisms to produce cosmic rays.

2.2 Solar Ejections

2.2.1 Solar Wind

The solar wind is defined as the plasma streaming out in all directions from the Sun's hot corona (Parker 1958) to the solar system and it makes up the interplanetary medium. The first evidence of the existence of the solar wind was from the Soviet spacecraft, Lunik III, and after that many observers can measure the details of the solar wind. From those data we know that the speed of the

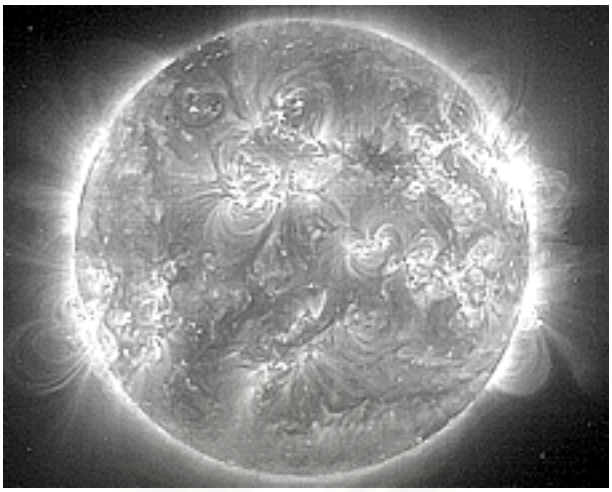

Figure 2.1: The image of solar flare on the sun is take in the EUV. In this figure we can see the magnetic loops. Areas of strong magnetic field are called active regions (http://coke.physics.ucla.edu/laptag/ VanNuys.dir/crs.htm).

solar wind is usually between 200 km/s to 800 km/s, while the sound speed in the solar wind near Earth is about 50 km/s (Cravens 1997). Variations in the solar wind speed can affect the Earth's magnetic field and create storms in the Earth's magnetosphere. The main components of the solar wind are protons, electrons, and He^{+2}. Other abundant ions are O^{+6}, Si^{+10}, N^{+5}, S^{+10}, and Si^{+9}, but these so-called minor ions form a small component of the solar wind plasma. Other quantities of the solar wind are its average proton density, about 7×10^6 m^{-3}, the average magnetic field, about 5×10^{-5} G, and the proton and electron temperatures of 0.4×10^5 K and 1.5×10^5 K, respectively.

2.2.2 Solar Flares

A solar flare is a sudden variation of brightness at the solar atmosphere. It occurs when a large magnetic loop (see in Figure 2.1) is built up on the Sun's surface and then an amount of particles, including protons, electrons, and heavy

nuclei, are heated, accelerated, and flow out into interplanetary space. The power release during a flare is typically on the order of 10^{27} ergs/s, though the total energy release can be up to 10^{33} ergs. One can roughly classify flares as impulsive or gradual events. Impulsive events have large e/p and high ^{3}He/^{4}He abundance ratios, while gradual events have low e/p and normal ^{3}He/^{4}He. Gradual events are generally associated with CME, and the particles that escape from the Sun are mainly accelerated at a CME-driven shock (Mason et al. 1984; Lee & Ryan 1986; Reames 1990; Ruffolo 1997). The rate of solar flare occurrences depends on the 11-year solar cycle.

The solar cycle is the cycle of activity on the Sun's surface. The period of high activity is called the solar maximum, while the quiet period of little activity is called the solar minimum. During solar maximum, there are many solar flares, CMEs, and sunspots, which are cooler areas that appear as dark points on the Sun's surface. The formation of sunspots occurs due to the emergence of magnetic field lines from the Sun's surface through the Sun's photosphere. Then we can observe the reconnection of the magnetic field lines above the sunspot when the solar flares and CMEs occur. The magnetic reconnection mainly converts potential energy to thermal energy in flares and kinetic energy in CMEs. The periodic variation of the sunspot number is shown in Figure 2.2.

2.2.3 Coronal Mass Ejections

Coronal Mass Ejections (CMEs) are events in which a huge mass of plasma is ejected from the sun, as shown in Figure 2.3. They are called coronal because the region of releasing plasma is the corona. The occurrence of coronal mass ejections is associated with solar flares and the number of CMEs depends on the solar cycle, too. The plasma in CMEs flows into interplanetary space with a

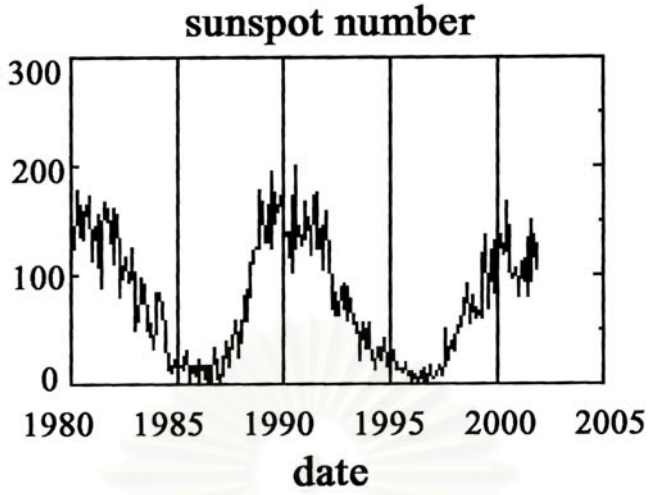

Figure 2.2: The number of sunspots observed during the last two solar cycles. A maximum occurred at around 1989, and the most recent came early in the year 2001 (http://www.sunspotcycle.com).

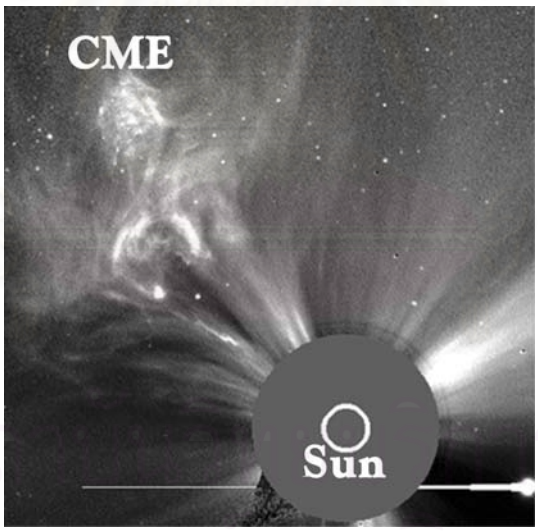

Figure 2.3: An image of a CME taken in soft X-rays. The huge mass is ejected from the Sun's surface (http://ens.lycos.com/ens/jun2000/2000L-06-08-09.html).

velocity of up to 2000 km/s, which is much larger than the solar wind velocity. The collision between these two plasmas of different velocities can cause a shock that accelerates particles in that region (see §2.5).

2.3 Interplanetary Magnetic Field

The interplanetary magnetic field is defined as the magnetic field from the Sun that is pulled from the Sun's surface by the solar wind into interplanetary space. Since the Sun rotates and has a continuous outflow of plasma, that makes the configuration of the magnetic field lines like that in Figure 2.4. From the data of the Pioneer, Voyager, and other spacecraft, we know that the magnetic field in space is not only from the Sun, but also from the planets such as Jupiter, Saturn, and Earth, too. The configuration of the planetary magnetic fields are not like those of the Sun. They have stable magnetic dipoles; an example of magnetic field lines near a planet is shown in Figure 2.5. The interaction between those magnetic field lines and the solar wind makes the solar energetic particles change trajectory and sometimes allows particle from the Sun to reach the Earth's atmosphere.

2.4 Charged Particle Motion along a Magnetic Field

We know that charged particles can move along a magnetic field line subject to the Lorentz force as shown in Figure 2.6. The orbit of a particle depends on the angle between the velocity of particle and the magnetic field, the pitch angle, θ. By convention, if $\theta > 90°$, the particle moves outward from the Sun, and when $\theta < 90°$, this particle will move toward the Sun. Since the irregularity of the

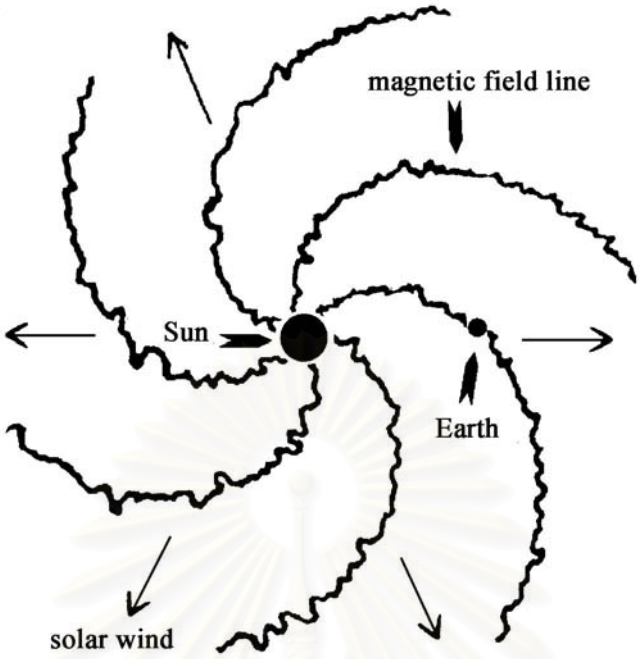

Figure 2.4: Illustration of the Sun and the magnetic field lines. The irregularity of the magnetic field occurs due to the turbulence of the solar wind (Parker 1958).

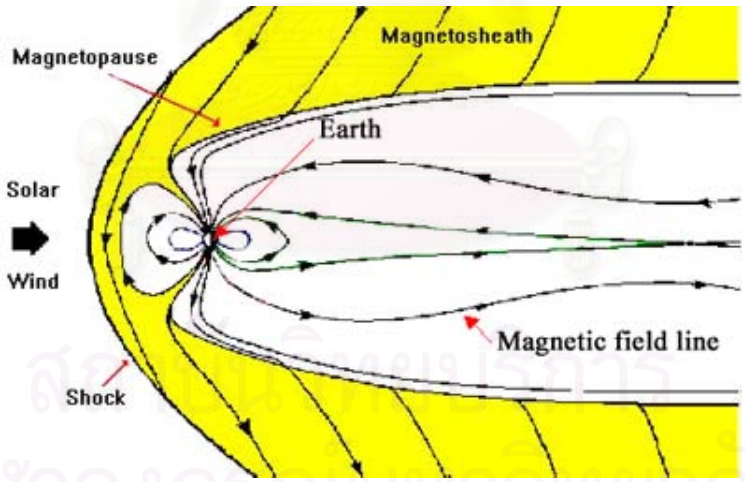

Figure 2.5: The Earth's magnetic field lines and the effect from the solar wind (http://www.oulu.fi/ spaceweb/textbook/fig/masphere.gif).

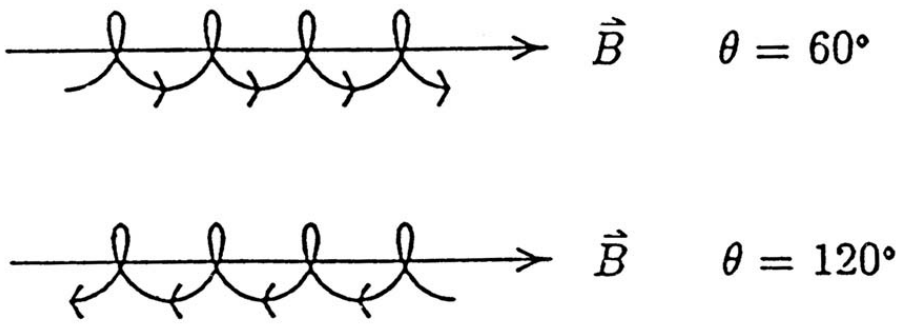

Figure 2.6: The trajectory of a particle along magnetic field line, depending on the pitch angle.

magnetic field from the Sun causes the changes in the pitch angles of particles, we say there is pitch angle scattering in the interplanetary medium.

2.5 Fermi Acceleration

The mechanism that is used to describe the acceleration of cosmic rays is the Fermi mechanism (Fermi 1949), which originally considered the interaction between magnetic field clouds and fast cosmic ray ions, such as protons. In this process, we assume that a proton has a spiral motion around the magnetic field, and can undergo reflection. The reflection of a particle can occur from two processes. In one process, known as "focusing" or "mirroring", when a particle moves in a region with a magnetic field gradient, the pitch angle changes so that the particle accelerates away from the strong field region. The second process, pitch angle scattering, involves random changes in the pitch angle, due to irregularities in the magnetic field.

To understand Fermi's model, we can visualize the reflection process as a collision between two masses (see Figure 2.7): the masses m and M refer

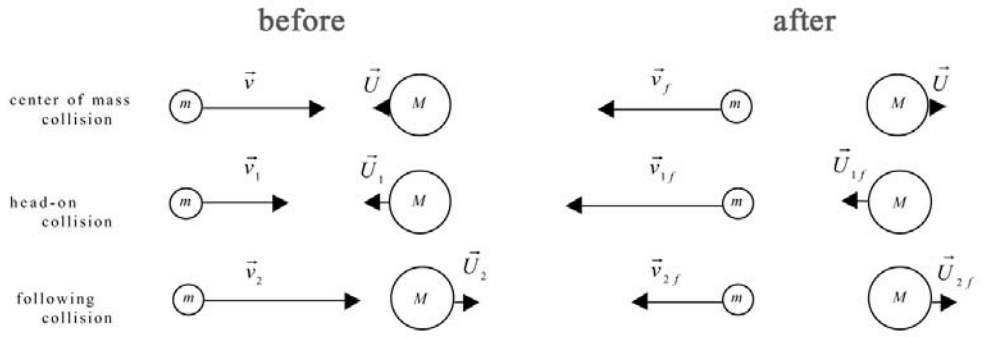

Figure 2.7: The elastic collision of particles m of velocity $\vec{v}$ and M of velocity $\vec{U}$ in three reference frames. The velocities before (no subscript) and after the collision (subscript f) are transformed into frames 1 and 2 to explain head-on and following collisions, respectively. Note that assuming $M \gg m$, then $U \approx 0$, $U_1 \approx U_{1f}$, $U_2 \approx U_{2f}$.

to the cosmic ray and the magnetic field structure responsible for the reflection, respectively. There are two types of collisions: a head-on collision and a following collision. Since the momentum and the energy are conserved in the center of mass frame, the magnitude of the velocity is constant in that frame, $\vec{v}_f = -\vec{v}$. The velocity after collision in each frame can be found from a transformation of the velocity from the center of mass frame to each frame. After transformation, the speed in the head-on collision frame is $v_1 = v - U_1$ before and $v_{1f} = v + U_1$ afterward, or increased by $2U_1$. The speed in the following frame is $v_2 = v + U_2$ before and $v_{2f} = v - U_2$ afterward, or decreased by $2U_2$.

First let us consider the case of random collisions. The average rate of gaining energy per collision of each type can be calculated using

$$\text{collision rate} = n\sigma v_{rel} \tag{2.1}$$

where n is the number density of particles, σ is the cross section, and v_{rel} is $v+U$

or $v - U$. For two quantities a and b related by

$$a = b^n,$$

we have

$$\frac{da}{a} = n\frac{db}{b}, \tag{2.2}$$

For a non-relativistic particle, $E = (1/2)mv^2$, so

$$\frac{dE}{E} = 2\frac{dv}{v} \tag{2.3}$$

We consider the average change in particle speed dv per collision:

$$\begin{aligned}
\langle dv \rangle &= \frac{(\text{following collision rate}) \cdot dv_2 + (\text{head-on collision rate}) \cdot dv_1}{(\text{total collision rate})} \\
&= \frac{n\sigma(v-U)(-2U) + n\sigma(v+U)(2U)}{n\sigma(v-U) + n\sigma(v+U)} \\
&= \frac{2n\sigma U^2 + 2n\sigma U^2}{2n\sigma v} \\
&= \frac{2U^2}{v}.
\end{aligned} \tag{2.4}$$

From (2.3) and (2.4), we get

$$\frac{dE}{E} = \frac{4U^2}{v^2}, \tag{2.5}$$

which is to second order in U/v. Therefore, this idea (Fermi 1949) is now called second-order Fermi acceleration. Note that $U \ll v$, so this acceleration process is not very efficient.

Another idea begins with a shock discontinuity in the magnetic field (de Hoffmann and Teller 1950), which occurs frequently in nature, where we consider

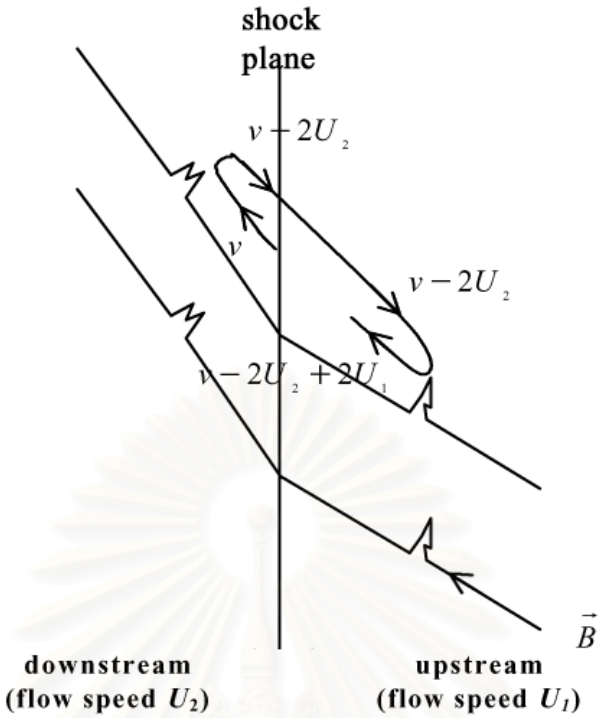

Figure 2.8: The particle velocity is changed after interacting with an irregularity in the of magnetic field. Such events occur both downstream and upstream.

the particle speed along the magnetic field. The large scale irregularities are compared with the mass M (see Figure 2.7), while the particle is compared with the mass m. The speed of irregularities upstream and downstream are U_1 (the upstream fluid speed) and U_2 (downstream fluid speed), respectively. Suppose that a particle reflects due to scattering both downstream (which is a region where the fluid has already passed the shock) and upstream (the region where the fluid has not passed), returning to its original position and orientation (Figure 2.8). After one cycle of a collision, the speed of the particle has changed by twice the difference between U_1 and U_2. The energy change per cycle in this case is found from

$$dv = dv_1 + dv_2,$$

$$= \quad 2\left(U_1 - U_2\right), \tag{2.6}$$

so

$$\frac{dE}{E} \quad = \quad \frac{4\left(U_1 - U_2\right)}{v}. \tag{2.7}$$

This energy gain, to first-order in U/v, is more efficient. This idea, now called first-order Fermi acceleration (Fermi 1954), is what we study in this work.

Chapter 3
Transport Equations

3.1 Fokker-Planck Equation

The Fokker-Planck Equation is a type of partial differential equation which is frequently used to describe the motion of particles that do not have collisions with other particles. The general form of this equation describes the time evolution of a probability distribution, which depends on variables such as time, spatial, or velocity coordinates. Then the fundamental Fokker-Planck equation is in the form (Wax 1954)

$$\frac{\partial F}{\partial t} + \frac{\partial}{\partial a_i}(\dot{a}_i F) = Q, \tag{3.1}$$

where $F = d^n N / \prod_i da_i$ is a function of time, t, and the variables $\{a_i\}$, N is the number of particles, Q is a source or second order term and $\dot{a}_i$ is the variation of a_i as a function of time. If the second-order term or source term goes to zero, we call this first-order linear equation the conservative form of the Fokker-Planck equation, which for example conserves of total number of particles. In this work we use the Fokker-Planck equation as the transport equation of cosmic rays in the continuous compression region. The equation that we are interested in is in terms of the distribution function, F, the distance, z, the momentum of a particle, p, the cosine of the pitch angle, μ, and time, t. Then from (3.1) we use a more specific form,

$$\frac{\partial F(t,\mu,z,p)}{\partial t} = -\frac{\partial}{\partial z}\left(\frac{\langle \Delta z \rangle}{\Delta t} F\right) - \frac{\partial}{\partial \mu}\left(\frac{\langle \Delta \mu \rangle}{\Delta t} F\right) - \frac{\partial}{\partial p}\left(\frac{\langle \Delta p \rangle}{\Delta t} F\right)$$

$$-\frac{\partial}{\partial\mu}\left[\frac{\varphi(\mu)}{2}\frac{\partial}{\partial\mu}\left(1-\frac{\mu\,v\,\vec{U}\cdot\hat{l}}{c^2}\right)F\right], \tag{3.2}$$

where $\varphi(\mu)$ is the pitch angle scattering coefficient as

$$\varphi(\mu) = a\,|\mu|^{q-1}\left(1-\mu^2\right), \tag{3.3}$$

a is the scattering amplitude, q controls the form of the scattering coefficient, v is the particle velocity, $\vec{U}$ is the solar wind velocity, c is the speed of light, $\hat{l}$ is the unit vector along the magnetic field line (Earl 1984; Ruffolo 1995), $F(t,\mu,z,p)$ is defined (Ng and Wong 1979) as

$$F(t,\mu,z,p) \equiv \frac{d^3N}{(d\mu dz dp)}, \tag{3.4}$$

N represents the number of particles inside a flux tube, and $\langle\Delta z\rangle/\Delta t$, $\langle\Delta\mu\rangle/\Delta t$, and $\langle\Delta p\rangle/\Delta t$ are the rate of change of a particle's position, pitch angle, and momentum in time, respectively. Furthermore, we will find the formulae to specify those values. In the remainder of this thesis the derivatives are taken to be operators, acting on *all* terms immediately to the right.

3.2 Cosmic Ray Transport Equation

The cosmic ray transport equation is adapted from previous work (Skilling 1971) by comparison and correction (Piyanate Chuychai 1999):

$$\frac{\langle\Delta\vec{x}\rangle}{\Delta t} = \vec{U} + \mu\,v\,\hat{l} - \frac{\mu^2 v^2 \vec{U}\cdot\hat{l}}{c^2}\,\hat{l}\,, \tag{3.5}$$

$$\frac{\langle\Delta\,p\rangle}{\Delta t} = p\left[\frac{1-3\mu^2}{2}\,l_i\,l_j\,\frac{\partial\,U_j}{\partial\,x_i} - \frac{1-\mu^2}{2}\vec{\nabla}\cdot\vec{U} - \frac{\mu}{v}\,\hat{l}\cdot\frac{\partial\,\vec{U}}{\partial t}\right], \tag{3.6}$$

$$\text{and} \qquad \frac{\langle \Delta\mu \rangle}{\Delta t} = \frac{1-\mu^2}{2}\left[v\,\vec{\nabla}\cdot\hat{l} + \mu\,\vec{\nabla}\cdot\vec{U} - 3\,\mu\,l_i\,l_j\,\frac{\partial\,U_j}{\partial\,x_i} + \frac{v\,\vec{U}}{c^2}\cdot\frac{\partial\,\hat{l}}{\partial\,t} \right.$$

$$\left. -\frac{2}{v}\,\hat{l}\cdot\frac{\partial\,\vec{U}}{\partial\,t} - \frac{\mu\,v^2\vec{U}\cdot\hat{l}}{c^2}\,\vec{\nabla}\cdot\hat{l} \right]. \qquad (3.7)$$

Then substituting the above equations into (3.2), we obtain the transport equation for the cosmic rays,

$$\frac{\partial F(t,z,\mu,p)}{\partial\,t} = -\frac{\partial}{\partial z}\left[U_z + \mu\,v\,l_z - \frac{\mu^2 v^2 \vec{U}\cdot\hat{l}}{c^2}\,l_z \right] F \qquad \text{streaming}$$

$$-\frac{\partial}{\partial\,p}\,p\left[\frac{1-3\mu^2}{2}\,l_i\,l_j\,\frac{\partial\,U_j}{\partial\,x_i} - \frac{1-\mu^2}{2}\vec{\nabla}\cdot\vec{U} - \frac{\mu}{v}\,\hat{l}\cdot\frac{\partial\,\vec{U}}{\partial\,t} \right] F$$

acceleration

$$-\frac{\partial}{\partial\mu}\frac{1-\mu^2}{2}\left[v\vec{\nabla}\cdot\hat{l} + \mu\vec{\nabla}\cdot\vec{U} - 3\mu\,l_i\,l_j\frac{\partial\,U_j}{\partial\,x_i} \right. \quad \text{focusing}$$

$$\left. +\frac{v\vec{U}}{c^2}\cdot\frac{\partial\,\hat{l}}{\partial\,t} - \frac{2}{v}\,\hat{l}\cdot\frac{\partial\,\vec{U}}{\partial\,t} - \frac{\mu\,v^2\vec{U}\cdot\hat{l}}{c^2}\,\vec{\nabla}\cdot\hat{l} \right] F$$

differential convection

$$+\frac{\partial}{\partial\mu}\left[\frac{\varphi(\mu)}{2}\frac{\partial}{\partial\mu}\left(1 - \frac{\mu\,v\,\vec{U}\cdot\hat{l}}{c^2} \right) F \right], \qquad \text{scattering} \qquad (3.8)$$

Each term on the right hand side of (3.8) corresponds to certain physical processes that affect F. The first term, which involves $\langle \Delta z \rangle / \Delta t$, is the streaming and convection term, describing how particles move along the direction z due to the velocity of the particles and velocity of the solar wind, respectively. The second term involves the deceleration or acceleration, depending on the physical situation, of particles (changes in momentum). In this work, we consider a compression of the fluid, so this term represents acceleration. The third and fourth

terms are focusing differential convection and scattering terms, which concern changes in pitch angle cosine, μ.

3.3 Model Configuration of the Magnetic Field in a Compression Region

The magnetic field line shape that is chosen for the compression is shown in Figure 3.1, which shows the structure of the magnetic field in 2 dimensions, in comparison with the shock case. Here $\vec{U}$ is the fluid (solar wind) velocity, and the subscripts 1 and 2 mean the upstream and downstream sides, respectively, while $\vec{B}$ is the magnetic field. Simulations are performed by using the configuration of hyperbolic magnetic field lines, in which the radius of curvature at $z = 0$ is adjusted though the value of $b/\lambda_{||}$; the radius of curvature $R = b \cot \theta_h$ where b is half of the conjugate axis, $\lambda_{||}$ is the scattering mean free path parallel to the field, and θ_h is parameter related to the upstream-to-downstream difference in the angle between the magnetic field and normal to the shock.

The function of the magnetic field line in this case is the function of a hyperbola which has a shape like in Figure 3.2. The equation which describes a hyperbola is

$$\frac{(y-k)^2}{a^2} - \frac{(x-h)^2}{b^2} = 1. \tag{3.9}$$

The asymptotic lines of this function, which are used to control the shape of the hyperbola, have the equations

$$y - k = \pm\frac{a}{b}(x-h). \tag{3.10}$$

The graph is adjusted to be appropriate for this work (Piyanate Chuychai 1999) by rotating the axes passing through the origin as in Figure 3.3. Then the

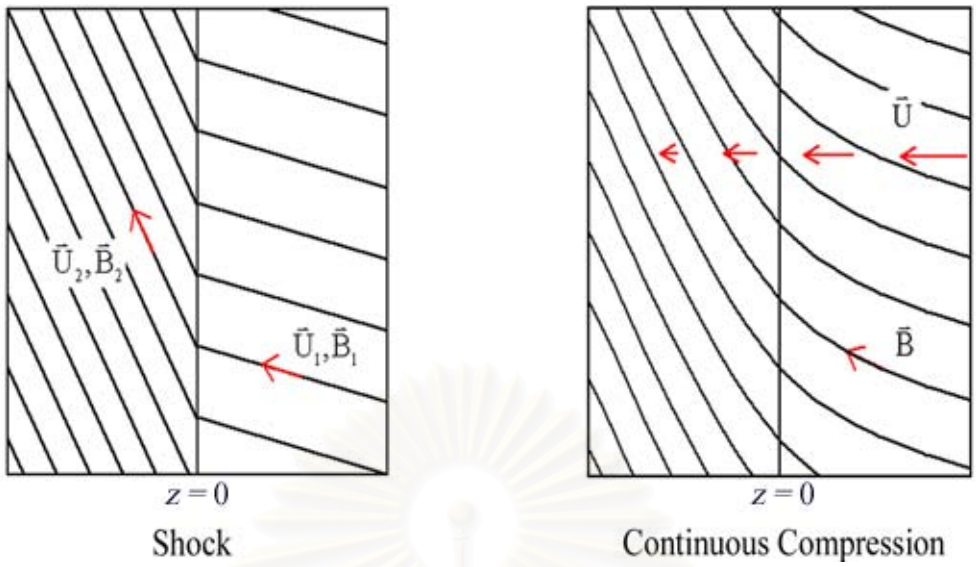

Figure 3.1: Model magnetic field configuration in the shock case and continuous compression case, respectively.

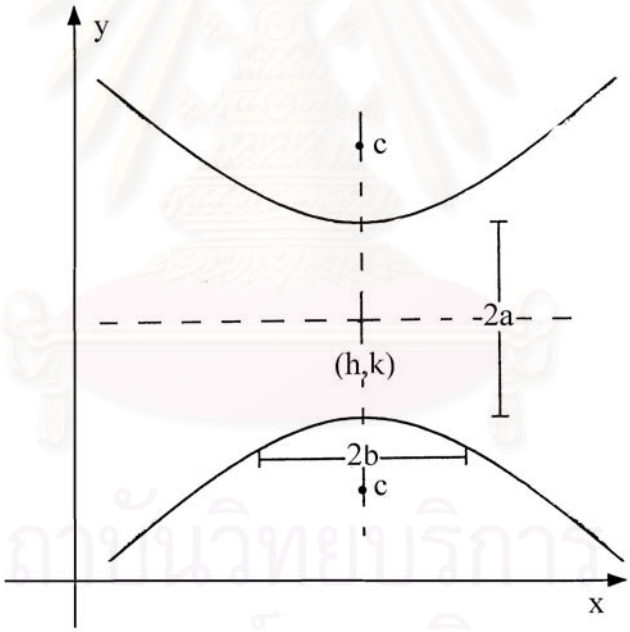

Figure 3.2: The graph of a hyperbola with center (h, k), the foci c, transverse axis $2a$, and conjugate axis $2b$. The conjugate axis of a hyperbola describes the width of the region of curvature; if b is small the curve is sharp.

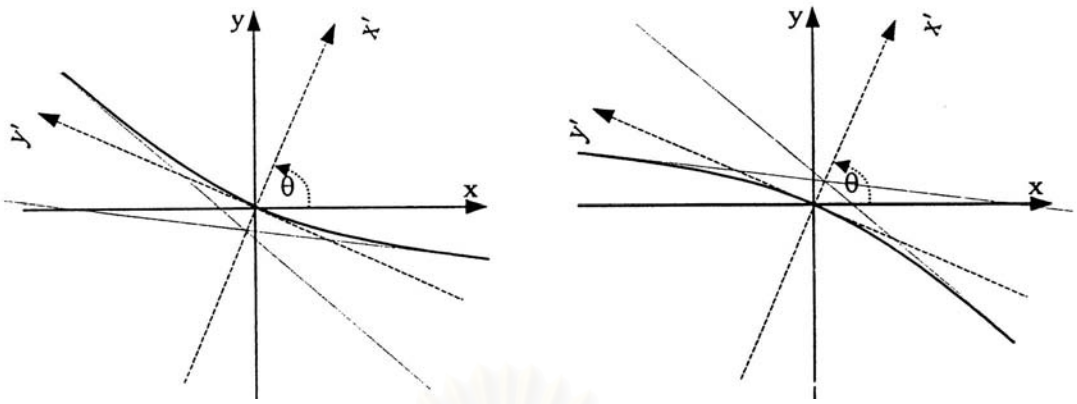

Figure 3.3: The hyperbolic graph after rotating the axes, for upper and lower branches, where θ is defined as the angle of rotation. In each case, the point of maximum curvature is shifted to the origin.

equation of this graph is given by

$$\frac{(y'-k)^2}{a^2} - \frac{(x'-h)^2}{b^2} = 1, \tag{3.11}$$

where the new coordinates (x', y') are related to the old coordinates (x, y) by the relations

$$x' = x\cos\theta + y\sin\theta, \qquad y' = -x\sin\theta + y\cos\theta, \tag{3.12}$$

and substituting equations (3.12) into (3.11) we will get the equation of the hyperbolic magnetic field line that we use:

$$\frac{(-x\sin\theta + y\cos\theta - k)^2}{a^2} - \frac{(x\cos\theta + y\sin\theta - h)^2}{b^2} = 1. \tag{3.13}$$

We know that this equation permits both branches of the graph, but in this work we choose only the upper branch for simulating, because of the similarity with the shock magnetic field that has been presented previously (Ruffolo 1999). The appropriate origin point is $(h, k) = (0, -a)$. Then equation (3.13) becomes

$$\frac{(-x\sin\theta + y\cos\theta + a)^2}{a^2} - \frac{(x\cos\theta + y\sin\theta)^2}{b^2} = 1. \tag{3.14}$$

The function, $y(x)$, can be found by solving the equation (3.14), which is quadratic in y, and then the solution is should be in the form

$$y(x) = \frac{-B + \sqrt{B^2 - 4AC}}{2A}, \tag{3.15}$$

where the constants A, B, and C are

$$\begin{aligned} A &= 1 - \sec^2\theta_h \sin^2\theta, \\ B &= -x^2 \sec^2\theta_h \sin 2\theta + 2b \tan\theta_h \cos\theta, \\ C &= x^2 \sec^2\theta_h \sin^2\theta - 2xb \tan\theta_h \sin\theta - x^2 \tan^2\theta_h, \end{aligned} \tag{3.16}$$

The parameters that we use in this work for describing the structure of the magnetic field are θ_h, b, the width of the region of curvature of the magnetic field line,

$$\theta_h = \frac{|\theta_1 - \theta_2|}{2}, \tag{3.17}$$

where in the upper branch case $\theta = (\theta_1 + \theta_h)$, because $\theta_1 < \theta_2$.

After the magnetic field line is determined, we apply this solution to find specific terms in the transport equation, which involve the unit vector along the magnetic field and solar wind, that is, $\hat{l}$ and $\vec{U}$. If $d\vec{s}$ is an infinitesimal distance along $\vec{B}$ then we obtain

$$d\vec{s} \times \vec{B} = 0. \tag{3.18}$$

Since we are interested in Cartesian coordinates,

$$\vec{B} = B_x\hat{x} + B_y\hat{y} + B_z\hat{z}, \tag{3.19}$$

the result of the cross product in equation (3.18) is

$$\frac{dx}{B_x} = \frac{dy}{B_y} = \frac{dz}{B_z}. \tag{3.20}$$

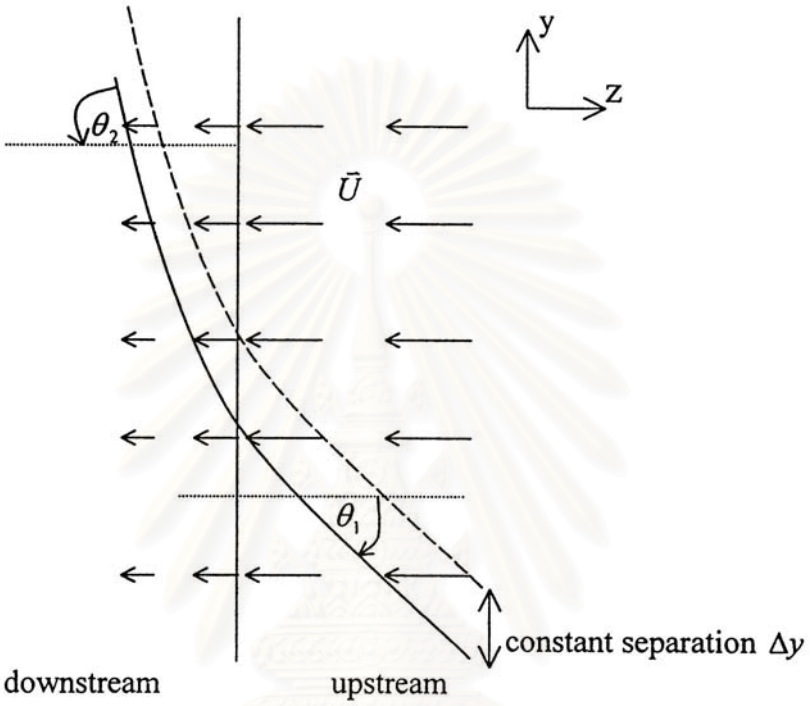

Figure 3.4: The structure of our model magnetic field compression, where the angle between magnetic field line and the compression normal on each side is different, $\theta_1 \neq \theta_2$; however, the flux tube size $\triangle y$ is constant. In addition, the solar wind velocity, assumed to be a vector along the z-axis, is not constant along z.

In this simulation we are interested in the magnetic field in two dimensions, (z, y), replacing x with z (see Figure 3.4), and then equation (3.20) is changed to

$$\frac{dy}{dz} = \frac{B_y}{B_z}, \tag{3.21}$$

or

$$B_y = \frac{dy}{dz} B_z. \tag{3.22}$$

Then equation (3.19) becomes

$$\vec{B} = B_z \left(\frac{dy}{dz} \hat{y} + \hat{z} \right). \tag{3.23}$$

Now we can find the unit vector along the magnetic field line, $\hat{l}$, by the relation

$$\hat{l} = \frac{\vec{B}}{|\vec{B}|}. \tag{3.24}$$

Then from equation (3.23) the magnitude of B is equal to

$$\begin{aligned} |\vec{B}| &= \sqrt{B_y^2 + B_z^2} \\ &= \sqrt{\left(\frac{dy}{dz}\right)^2 B_z^2 + B_z^2}. \end{aligned} \tag{3.25}$$

Substituting (3.23) and (3.25) into (3.24), we get

$$\hat{l} = \frac{dy/dz}{\sqrt{1 + (dy/dz)^2}} \hat{y} + \frac{1}{\sqrt{1 + (dy/dz)^2}} \hat{z} \ . \tag{3.26}$$

From Figure 3.4, we see that the solar wind velocity, $\vec{U}$, is changing. A decrease in $\vec{U}$ along the flow is called a "compression," i.e., two streams of fluid have a relative velocity toward each other. The reason is that while the solar wind is ejected from the sun it drag the magnetic field lines to the interplanetary space, in the same time the plasma in solar wind is followed along magnetic field. Then

the changes in the two quantities are interdependent. In this work we assume that

$$\vec{U} = U_z \hat{z}, \tag{3.27}$$

and the relation between the magnetic field line and solar wind velocity is assumed to be

$$U_z \propto \frac{dz}{dy} \quad \text{or} \quad U_z = \frac{c}{dy/dz}\ , \tag{3.28}$$

so

$$c = U_z \cdot \frac{dy}{dz}. \tag{3.29}$$

The constant c can be found by the boundary condition. If the solar wind speed far upstream is set to $-U_{1n}$ and $dy/dz = -\tan\theta_1$, then $c = -U_{1n} \cdot (\tan\theta_1)$ and equation (3.27) becomes

$$\vec{U} = \frac{-U_{1n} \cdot \tan\theta_1}{dy/dz}\,\hat{z}. \tag{3.30}$$

Now we have the parameters that involve the magnetic field line in the compression region already, and next specific terms in the transport equation are derived as follows:

$$l_z = \frac{1}{\sqrt{1 + (dy/dz)^2}}\,, \tag{3.31}$$

(3.32)

$$U_z = \frac{-U_{1n} \cdot \tan\theta_1}{dy/dz}\,, \tag{3.33}$$

(3.34)

$$\begin{aligned} \vec{U} \cdot \hat{l} &= U_z l_z \\ &= \frac{-U_{1n}\ \tan\theta_1}{dy/dz} \cdot \frac{1}{\sqrt{1 + (dy/dz)^2}}\,, \end{aligned} \tag{3.35}$$

(3.36)

$$\vec{\nabla}\cdot\hat{l} = \frac{\partial l_z}{\partial z}$$
$$= -\frac{dy}{dz}\cdot\frac{d^2y}{d\,z^2}\cdot {l_z}^3\,, \tag{3.37}$$
$$\tag{3.38}$$
$$\vec{\nabla}\cdot\vec{U} = \frac{\partial U_z}{\partial z}$$
$$= \frac{U_{1n}\tan\theta_1}{(dy/dz)^2}\cdot\frac{d^2y}{d\,z^2}\,, \tag{3.39}$$
$$\tag{3.40}$$
$$l_i\,l_j\,\frac{\partial U_j}{\partial x_i} = l_z\,l_z\,\frac{\partial U_z}{\partial z}$$
$$= l_z^2\left(\frac{U_{1n}\,\tan\theta_1}{(dy/dz)^2}\cdot\frac{d^2y}{d\,z^2}\right)\,, \tag{3.41}$$

where in our model gradients are non-zero only in the z-direction. Since both $\vec{U}$ and $\hat{l}$ do not depend on time,

$$\vec{U}\cdot\frac{\partial\hat{l}}{\partial t} = 0\,, \tag{3.42}$$
$$\hat{l}\cdot\frac{\partial\vec{U}}{\partial t} = 0\,. \tag{3.43}$$

The terms dy/dz and d^2y/dz^2 can be found by using the configuration of the magnetic field following equations (3.15) and (3.16). As a result we can solve the transport equation by numerical techniques as described in Chapter 4.

3.4 Diffusion-Convection Equation

The diffusion-convection equation is widely used to study the propagation of particles. The general form of this equation is

$$\frac{\partial F}{\partial t} = -\frac{\partial S}{\partial z}, \tag{3.44}$$

where F is the particle density, S is the flux of particle density,

$$S = UF - D\frac{\partial F}{\partial z} \tag{3.45}$$

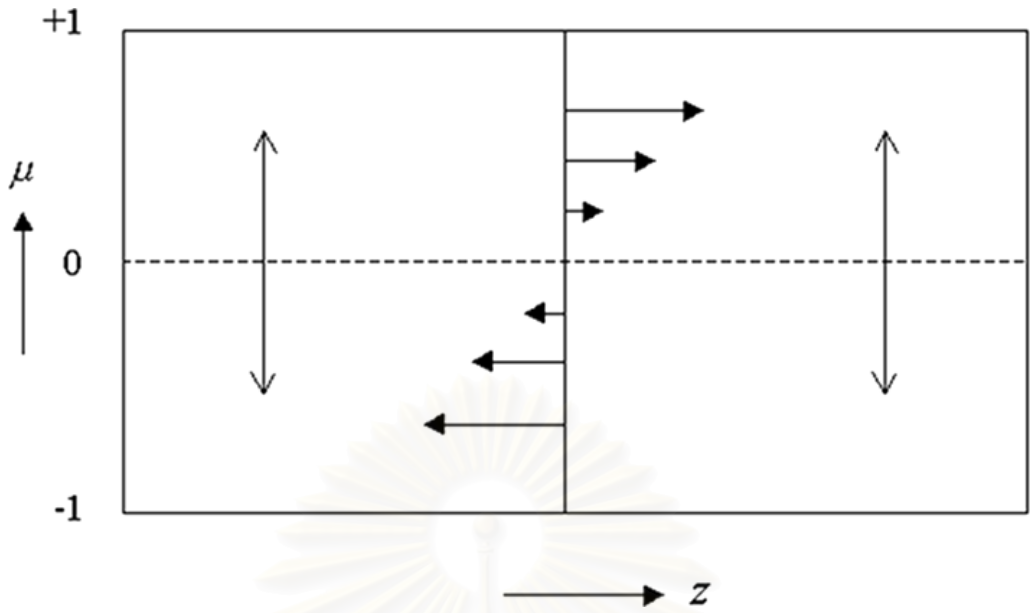

Figure 3.5: The pitch angle scattering makes particles undergo a random walk in μ, the pitch angle cosine, moving up and down in this graph, while the streaming velocity along z is $v\cos\theta$ or μv.

which is composed of two terms. One is the convective term, UF, and the other is the diffusive term, $-D\,\partial F/\partial z$, which is related to Fick's Law, where D is the diffusion coefficient. The transformation from the pitch angle transport equation that we use to the diffusion-convection equation uses the so-called diffusion approximation.

We start by considering the particle motion in μ and z, as shown in Figure 3.5 (not considering momentum changes at the moment). The particle density is in the form $F(t, z, \mu)$. The effect of pitch angle scattering on the particle density is shown in Figures 3.5 and 3.6. We see that if the distribution in μ is nearly isotropic, the pitch angle scattering implies a random walk in z, and we have a diffusive process with a small and nearly constant anisotropy (μ-dependence) of the particle density. Earl (1974) described the distribution function for charged

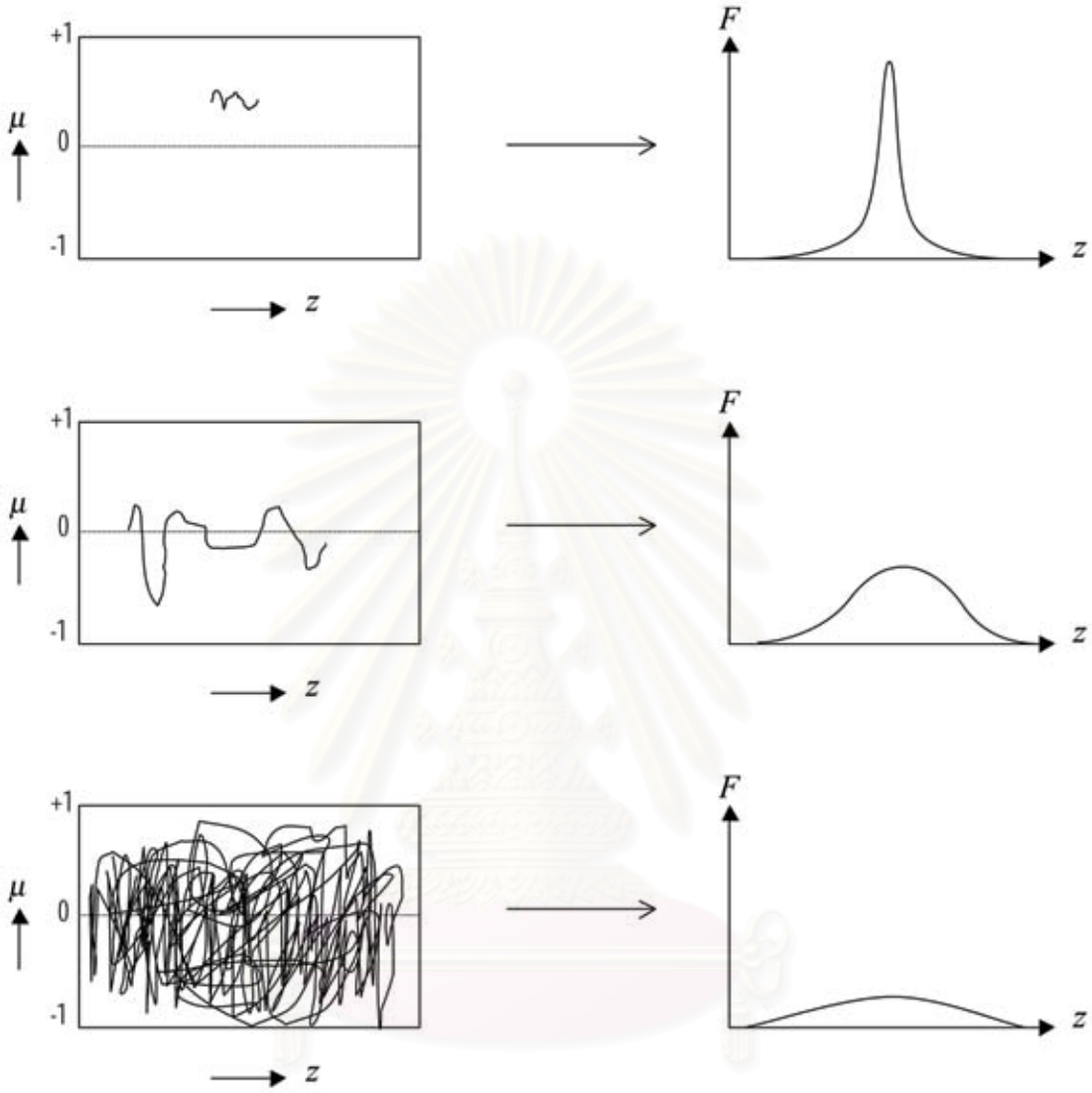

Figure 3.6: The particle density depends on changes in μ. We assume that particles start at the same (μ, z) coordinates. If μ has not changed much, the particle density, F, has a sharp shape, but if μ has changed greatly (due to scattering, a random walk in μ), F will spread out diffusively in z.

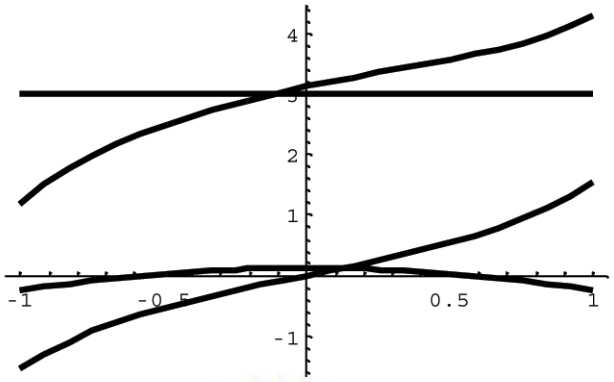

Figure 3.7: A rough illustration of F as a summation of F_0, F_1, and F_2.

particles diffusing along a magnetic field line by this diffusion approximation. We applied this derivation to our transport equation by approximating

$$F(t,\mu,p,z) \approx F_0(t,p,z) + F_1(\mu,p,z) + F_2(\mu,p,z), \tag{3.46}$$

where $F_0 \equiv \langle F \rangle_\mu$, F_1 is an odd function of μ, and F_2 is an even function of μ, as illustrated in Figure 3.7. The F_2 function does not lead to a strong flux, so its effect is neglected in this approximation. The form of 3.46 implies some assumptions:

- $F(\mu)$ is nearly constant,
- $|\partial F_1/\partial t| \ll |\mu v \partial F_0/\partial z|$,
- $|U_{1n}\partial F_1/\partial z| \ll |\mu v \partial F_0/\partial z|$.

We substitute (3.46) into (3.8), and then the result is split into even and odd terms. The even terms give

$$\frac{\partial F_0}{\partial t} = -\frac{\partial}{\partial z}\left[U_z - \frac{\mu^2 v^2 \vec{U}\cdot\hat{l}}{c^2} l_z\right] F_0 - \frac{\partial}{\partial z}\left(\mu v l_z\right) F_1$$

$$-\frac{\partial}{\partial p} p\left[\left(\frac{1-3\mu^2}{2}\right) l_i l_j \frac{\partial U_j}{\partial x_i} - \left(\frac{1-\mu^2}{2}\right) \vec{\nabla}\cdot\vec{U}\right] F_0 + \frac{\partial}{\partial p}\left(\frac{\mu}{v}\hat{l}\cdot\frac{\partial \vec{U}}{\partial t}\right) F_1$$

$$-\frac{\partial}{\partial\mu}\left(\frac{1-\mu^2}{2}\right)\left[-3\mu l_i l_j\frac{\partial U_j}{\partial x_i}+\mu\vec{\nabla}\cdot\vec{U}-\frac{\mu v^2\vec{U}\cdot\hat{l}}{c^2}\vec{\nabla}\cdot\hat{l}\right]F_0$$

$$-\frac{\partial}{\partial\mu}\left(\frac{1-\mu^2}{2}\right)\left[v\vec{\nabla}\cdot\hat{l}+\frac{v\vec{U}}{c^2}\cdot\frac{\partial\hat{l}}{\partial t}-\frac{2}{v}\hat{l}\cdot\frac{\partial\vec{U}}{\partial t}\right]F_1$$

$$+\frac{\partial}{\partial\mu}\frac{\varphi(\mu)}{2}\frac{\partial F_0}{\partial\mu}-\frac{\partial}{\partial\mu}\frac{\varphi(\mu)}{2}\frac{\partial}{\partial\mu}\frac{\mu v\vec{U}\cdot\hat{l}}{c^2}F_1, \tag{3.47}$$

and the odd terms are

$$\begin{aligned}\frac{\partial F_1}{\partial t} &= -\frac{\partial}{\partial z}\left[U_z-\frac{\mu^2v^2\vec{U}\cdot\hat{l}}{c^2}l_z\right]F_1-\frac{\partial}{\partial z}\left(\mu v l_z\right)F_0\\
&\quad -\frac{\partial}{\partial p}p\left[\left(\frac{1-3\mu^2}{2}\right)l_il_j\frac{\partial U_j}{\partial x_i}-\left(\frac{1-\mu^2}{2}\right)\vec{\nabla}\cdot\vec{U}\right]F_1+\frac{\partial}{\partial p}\frac{\mu}{v}\hat{l}\cdot\frac{\partial\vec{U}}{\partial t}F_0\\
&\quad -\frac{\partial}{\partial\mu}\left(\frac{1-\mu^2}{2}\right)\left[-3\mu l_il_j\frac{\partial U_j}{\partial x_i}+\mu\vec{\nabla}\cdot\vec{U}-\frac{\mu v^2\vec{U}\cdot\hat{l}}{c^2}\vec{\nabla}\cdot\hat{l}\right]F_1\\
&\quad -\frac{\partial}{\partial\mu}\left(\frac{1-\mu^2}{2}\right)\left[v\vec{\nabla}\cdot\hat{l}+\frac{v\vec{U}}{c^2}\cdot\frac{\partial\hat{l}}{\partial t}-\frac{2}{v}\hat{l}\cdot\frac{\partial\vec{U}}{\partial t}\right]F_0\\
&\quad +\frac{\partial}{\partial\mu}\frac{\varphi(\mu)}{2}\frac{\partial F_1}{\partial\mu}-\frac{\partial}{\partial\mu}\frac{\varphi(\mu)}{2}\frac{\partial}{\partial\mu}\frac{\mu v\vec{U}\cdot\hat{l}}{c^2}F_0.\end{aligned} \tag{3.48}$$

We want an equation that is independent of μ, so we average the odd and even terms over μ.

Some results that are used to solve the integrals are:

$$\begin{aligned}\frac{1}{2}\int_{-1}^{1}\mu^2d\mu &= \frac{1}{3},\\
\frac{1}{2}\int_{-1}^{1}\mu d\mu &= 0,\\
\frac{1}{2}\int_{-1}^{1}\left(\frac{1-3\mu^2}{2}\right)d\mu &= 0,\\
\frac{1}{2}\int_{-1}^{1}\left(\frac{1-\mu^2}{2}\right)d\mu &= \frac{1}{3},\end{aligned}$$

$$\begin{aligned}
\frac{1}{2}\int_{-1}^{1}\frac{\partial}{\partial\mu}\mu\left(\frac{1-\mu^2}{2}\right)d\mu &= 0,\\
\frac{1}{2}\int_{-1}^{1}\frac{\partial}{\partial\mu}\left(\frac{1-\mu^2}{2}\right)d\mu &= 0,\\
\frac{1}{2}\int_{-1}^{1}\frac{\partial}{\partial\mu}\frac{\varphi(\mu)}{2}\frac{\partial F_0}{\partial\mu}d\mu &= 0, \qquad (3.49)
\end{aligned}$$

where we recall that F_0 is independent of μ. Then equation (3.47) becomes

$$\begin{aligned}
\frac{\partial F_0}{\partial t} &= -\frac{\partial}{\partial z}\left[U_z-\frac{1}{3}\frac{v^2\vec{U}\cdot\hat{l}}{c^2}l_z\right]F_0-\frac{\partial}{\partial z}vl_z\frac{1}{2}\int_{-1}^{1}\mu F_1 d\mu\\
&\quad+\frac{1}{3}\vec{\nabla}\cdot\vec{U}\frac{\partial}{\partial p}pF_0+\frac{\partial}{\partial p}p\left(\frac{\hat{l}}{v}\cdot\frac{\partial\vec{U}}{\partial t}\right)\frac{1}{2}\int_{-1}^{1}\mu F_1 d\mu.
\end{aligned}$$

Comparing between equation (3.50) and the diffusion-convection equation (3.44), we can write

$$\frac{\partial F_0}{\partial t} = -\frac{\partial S}{\partial z}+\frac{\partial}{\partial p}\frac{p}{3}(\vec{\nabla}\cdot\vec{U})F_0+\frac{\partial}{\partial p}\left(\frac{\hat{l}}{v}\cdot\frac{\partial\vec{U}}{\partial t}\right)\frac{1}{2}\int_{-1}^{1}\mu F_1 d\mu, \qquad (3.50)$$

where

$$S = \left[U_z-\frac{1}{3}\frac{v^2\vec{U}\cdot\hat{l}}{c^2}l_z\right]F_0+vl_z\frac{1}{2}\int_{-1}^{1}\mu F_1 d\mu. \qquad (3.51)$$

Now we want to eliminate F_1 by finding F_1 in terms of F_0. We start by integrating (3.48) over μ from -1 to ν. Then we set the left hand side to zero, recalling our assumption that $\partial F_1/\partial t$ is negligible. The results from integrating are

$$\begin{aligned}
\int_{-1}^{\nu}\mu d\mu &= -\frac{1-\nu^2}{2},\\
\int_{-1}^{\nu}\frac{\partial}{\partial\mu}\left(\frac{1-\mu^2}{2}\right)\mu F_1 d\mu &= \frac{1-\nu^2}{2}\nu F_1(\nu),\\
\int_{-1}^{\nu}\frac{\partial}{\partial\mu}\left(\frac{1-\mu^2}{2}\right)F_1 d\mu &= \frac{1-\nu^2}{2}F_1(\nu),
\end{aligned}$$

$$\int_{-1}^{\nu}\frac{\partial}{\partial\mu}\frac{\varphi(\mu)}{2}\frac{\partial F_1}{\partial\mu}d\mu = \frac{\varphi(\nu)}{2}\frac{\partial F_1(\nu)}{\partial\nu},$$
$$\int_{-1}^{\nu}\frac{\partial}{\partial\mu}\frac{\varphi(\mu)}{2}\frac{\partial\mu}{\partial\mu}d\mu = \frac{\varphi(\nu)}{2}. \tag{3.52}$$

We can neglect $\partial F_1/\partial t$ and $\partial F_1/\partial z$, so the result is

$$\begin{aligned}0 = {} & \left(\frac{1-\nu^2}{2}\right)v\frac{\partial}{\partial z}l_zF_0 - \frac{\partial}{\partial p}p\left(\frac{1-\nu^2}{2}\right)\frac{\hat{l}}{v}\cdot\frac{\partial\vec{U}}{\partial t}F_0 \\ & -\left(\frac{1-\nu^2}{2}\right)\left(v\vec{\nabla}\cdot\hat{l}+\frac{v\vec{U}}{c^2}\cdot\frac{\partial\hat{l}}{\partial t}-\frac{2\hat{l}}{v}\cdot\frac{\partial\vec{U}}{\partial t}\right)F_0 \\ & +\frac{\varphi(\nu)}{2}\frac{\partial F_1(\nu)}{\partial\nu}-\frac{v\vec{U}\cdot\hat{l}}{c^2}\frac{\varphi(\nu)}{2}F_0,\end{aligned} \tag{3.53}$$

and we use the relation

$$\frac{\partial}{\partial z}(l_zF_0) = l_z\frac{\partial F_0}{\partial z}+F_0\frac{\partial l_z}{\partial z},$$

to simplify (3.53). Moreover, we set the solar wind vector and the unit vector along the magnetic field to be constant in time. Then $\partial F_1/\partial\nu$ is found in the form

$$\begin{aligned}\frac{\partial F_1(\nu)}{\partial\nu} = {} & -\left[\frac{1-\nu^2}{\varphi(\nu)}\right]vl_z\frac{\partial F_0}{\partial z}+\left[\frac{1-\nu^2}{\varphi(\nu)}\right]v\left(\vec{\nabla}\cdot\hat{l}-\frac{\partial l_z}{\partial z}\right)F_0 \\ & +\frac{v\vec{U}\cdot\hat{l}}{c^2}F_0,\end{aligned} \tag{3.54}$$

and we have

$$\begin{aligned}\int_0^{\mu}dF_1(\nu) = {} & -\left\{\int_0^{\mu}\left[\frac{1-\nu^2}{\varphi(\nu)}\right]d\nu\right\}vl_z\frac{\partial F_0}{\partial z}+\left\{\int_0^{\mu}\left[\frac{1-\nu^2}{\varphi(\nu)}\right]d\nu\right\} \\ & \times v\left(\vec{\nabla}\cdot\hat{l}-\frac{\partial l_z}{\partial z}\right)F_0+\left(\int_0^{\mu}d\nu\right)\frac{v\vec{U}\cdot\hat{l}}{c^2}F_0,\end{aligned} \tag{3.55}$$

$$F_1(\mu) = -\left\{\int_0^\mu \left[\frac{1-\nu^2}{\varphi(\nu)}\right] d\nu\right\} v l_z \frac{\partial F_0}{\partial z} + \left\{\int_0^\mu \left[\frac{1-\nu^2}{\varphi(\nu)}\right] d\nu\right\} v \left(\vec{\nabla}\cdot\hat{l} - \frac{\partial l_z}{\partial z}\right) F_0$$
$$+\frac{\mu v \vec{U}\cdot\hat{l}}{c^2} F_0. \tag{3.56}$$

Substituting (3.56) into (3.51) we get

$$\begin{aligned} S &= \left[U_z - \frac{1}{3}\frac{v^2\vec{U}\cdot\hat{l}}{c^2}\right] F_0 + v l_z \frac{1}{2}\left\{\int_{-1}^1 \mu(-v l_z)\int_0^\mu \left[\frac{1-\nu^2}{\varphi(\nu)}\right] d\nu d\mu\right\}\frac{\partial F_0}{\partial z} \\ &\quad + v l_z \frac{1}{2}\left\{\int_{-1}^1 \mu\left[+v\left(\vec{\nabla}\cdot\hat{l} - \frac{\partial l_z}{\partial z}\right)\right]\int_0^\mu \left[\frac{(1-\nu^2)}{\varphi(\nu)}\right] d\nu d\mu\right\} F_0 \\ &\quad + v l_z \frac{1}{2}\left[\int_{-1}^1 \left(\frac{\mu^2 v\vec{U}\cdot\hat{l}}{c^2}\right) d\mu\right] F_0, \\ &= U_z F_0 - v^2 l_z^2 \frac{1}{2}\left\{\int_{-1}^1\int_0^\mu \mu\left[\frac{1-\nu^2}{\varphi(\nu)}\right] d\nu d\mu\right\}\frac{\partial F_0}{\partial z} \\ &\quad + \frac{v^2 l_z^2}{l_z}\frac{1}{2}\left\{\int_{-1}^1\int_0^\mu \mu\left[\frac{1-\nu^2}{\varphi(\nu)}\right] d\nu d\mu\right\} F_0\left(\vec{\nabla}\cdot\hat{l} - \frac{\partial l_z}{\partial z}\right), \end{aligned} \tag{3.57}$$

and using integration by parts,

$$\begin{aligned} S &= U_z F_0 - v^2 l_z^2 \frac{1}{4}\left[\int_{-1}^1 \frac{(1-\mu^2)^2}{\varphi(\mu)} d\mu\right]\frac{\partial F_0}{\partial z} \\ &\quad + \frac{v^2 l_z^2}{l_z}\frac{1}{4}\left[\int_{-1}^1 \frac{(1-\mu^2)^2}{\varphi(\mu)} d\mu\right] F_0\left(\vec{\nabla}\cdot\hat{l} - \frac{\partial l_z}{\partial z}\right), \\ &= U_z F_0 - D\frac{\partial F_0}{\partial z} + \frac{D}{l_z} F_0\left(\vec{\nabla}\cdot\hat{l} - \frac{\partial l_z}{\partial z}\right), \end{aligned} \tag{3.58}$$

where

$$D = v^2 l_z^2 \frac{1}{4}\int_{-1}^1 \frac{(1-\mu^2)^2}{\varphi(\mu)} d\mu$$

is the spatial diffusion coefficient (in z). We can write S in the form:

$$S = U_z F_0 - D\frac{\partial F_0}{\partial z} + \frac{D}{l_z} F_0\left(\frac{\partial l_x}{\partial x} + \frac{\partial l_y}{\partial y}\right)$$

$$= \quad U_z F_0 - D\frac{\partial F_0}{\partial z} + DF_0 \frac{1}{A}\frac{dA}{dz}, \tag{3.59}$$

where A is the cross-sectional area of flux tube, and perpendicular to $\vec{B}$ (and $\hat{l}$).

The equation (3.59) can be expressed in terms of an observed intensity, j, where

$$j \quad = \quad \frac{d^6 N}{d^3 x dp d\Omega}. \tag{3.60}$$

The definition of F (equation 3.4) and j (equation 3.60) is related by

$$F_0 = 2\pi A j \tag{3.61}$$

(assuming a uniform distribution in the gyrophase). Using the logarithmic derivative, which is

$$\begin{aligned} \frac{1}{F_0}\frac{dF_0}{dz} &= \frac{d}{dz}(\ln F_0) \\ &= \frac{d}{dz}(\ln A) + \frac{d}{dz}(\ln j) \qquad (3.62) \\ &= \frac{1}{A}\frac{dA}{dz} + \frac{1}{j}\frac{dj}{dz}, \qquad (3.63) \end{aligned}$$

we write equation (3.59) in terms of j.

$$S \quad = \quad U_z F_0 - D\frac{F_0}{j}\frac{\partial j}{\partial z}. \tag{3.64}$$

Finally we assume $F_0 \propto p^{-\gamma}$ (at least locally), to obtained a diffusion-convection equation in the steady-state ($dF_0/dt = 0$):

$$\frac{d}{dz}D\frac{F_0}{j}\frac{dj}{dz} - \frac{d}{dz}U_z F_0 - \frac{\gamma - 1}{3}(\vec{\nabla}\cdot\vec{U})F_0 = 0. \tag{3.65}$$

3.5 Analytic Solutions for Special Cases

Referring to Figure 3.1, the magnetic fields far upstream or far downstream of a compression and a shock are not different. Then the boundary condition for a compression can be considered from the boundary condition for a shock (Ruffolo 1999), which is designed to match the solution of the diffusion-convection equation (e.g., Krymskii 1977). The diffusion approximation should be valid far from the shock or compression.

The diffusion-convection equation for a shock is

$$\frac{\partial F_0}{\partial t} = -\frac{\partial S}{\partial z}, \tag{3.66}$$

where

$$S = UF_0 - D\frac{\partial F_0}{\partial z} \tag{3.67}$$

on one side of the shock (upstream or downstream), where U is constant, and U is the fluid speed along z. In our work we define $z > 0$ to be upstream, so we use $U < 0$. Note that we define z along the shock normal, so $A(z)$ is constant and F_0 and j are interchangeable in our work. In the steady-state, equation (3.67) requires that S be constant on either side of the shock, so the solution is

$$F_0 = c_1 + c_2 \exp\left(\frac{U}{D}z\right), \tag{3.68}$$

where c_1 and c_2 are constants. Downstream ($z < 0$), c_2 is set to zero, in order to avoid divergence; then $\partial F_0/\partial z = 0$ and F_0 is constant. Far upstream, we assume that there is a negligible flux of energetic particles, so we set $c_1 = 0$, and F_0 decays exponentially in z.

Furthermore, we consider the anisotropy of F_0 by examining equation (3.54). In this work, we consider isotropic scattering, so $q = 1$. The pitch angle

coefficient is in the form of $\varphi(\nu) = a(1-\nu^2)$ (see equation 3.3). Then equation (3.54) becomes

$$\frac{\partial F_1(\nu)}{\partial \nu} = -\frac{vl_z}{a}\frac{\partial F_0}{\partial z} - \frac{v}{a}\left(\vec{\nabla}\cdot\hat{l} - \frac{\partial l_z}{\partial z}\right)F_0 + \frac{v\vec{U}\cdot\hat{l}}{c^2}F_0. \tag{3.69}$$

Now the right hand side of equation (3.69) does not include the variable ν. This means that $F_1(\nu) = \delta \cdot F_0 \cdot \nu$, where δ is called the anisotropy of F_0.

We find δ from consideration of equation (3.51). Changing ν to μ, we have

$$S = \left[U_z - \frac{v^2\vec{U}\cdot\hat{l}}{3c^2}l_z\right]F_0 + \frac{vl_z\delta}{3}F_0. \tag{3.70}$$

Comparing equations (3.70) and (3.64), and recalling that F_0/j is constant, we have

$$\frac{vl_z}{3}\left[\delta - \frac{v\vec{U}\cdot\hat{l}}{c^2}\right]F_0 = -D\frac{\partial F_0}{\partial z}, \tag{3.71}$$

$$\delta = -\frac{3D}{vl_zF_0}\frac{\partial F_0}{\partial z} + \frac{v\vec{U}\cdot\hat{l}}{c^2}. \tag{3.72}$$

Recall that far downstream, $\partial F_0/\partial z$ equal to zero (to avoid divergence as $z \to -\infty$), so

$$\delta = \frac{\vec{U}\cdot\hat{l}v}{c^2}, \tag{3.73}$$

$$= \frac{U_z l_z v}{c^2}. \tag{3.74}$$

Since far upstream,

$$\frac{\partial F_0}{\partial z} = \frac{U_z}{D}F_0, \tag{3.75}$$

then the expected value of δ far upstream is

$$\delta = -\frac{3U_z}{vl_z} + \frac{U_z l_z v}{c^2}, \tag{3.76}$$

which depends on the fluid speed and the particle momentum.

In this work, we calculate the δ by using $U_z = 544.3$ km/s$^{-1} = 0.001816 \times c$ and for $v/U_z = 10$ or 50. The results from this analytic calculation (which is only valid far from the shock or compression) and the full simulations are compared in Chapter 5 .

Chapter 4
Numerical Techniques

4.1 Existing Numerical Techniques

In the simulation work, we use three methods to solve the transport equation. Each method depends on the variables (z, μ, p) and the boundary values.

4.1.1 Crank-Nicolson Finite Difference

This method is used to solve the transport equation in terms of μ. Before going into details of the Crank-Nicolson finite difference method, we will introduce some simpler examples of finite differencing. Suppose we have a function $y(x)$ and we want to find the value of this function along x by the approximation $y_i \approx y(x_i)$, where $x_i \in [a, b]$ are discrete. Then we set $x_0 = a$, $x_1 = a + \Delta x$, $x_2 = a + 2\Delta x$, ..., $x_N = a + N\Delta x = b$, where N is the number of intervals Δx. The ordinary differential of $y(x)$ is dy/dx, which can be estimated by the finite difference method in three ways:

1. Forward differences:

$$\left.\frac{dy}{dx}\right|_{x_i} \approx \frac{y_{i+1} - y_i}{\Delta x}. \tag{4.1}$$

The error of this approximation can be found by a Taylor series expansion. We replace y_i, y_{i-1}, y_{i+1} by $y(x_i)$, $y(x_{i-1})$, $y(x_{i+1})$, respectively. Then equation (4.1) is given by

$$y(x_{i+1}) - y(x_i) \;=\; y(x_i) + y'(x_i)\Delta x + \frac{1}{2}y''(x_i)(\Delta x)^2 + \ldots - y(x_i),$$

$$\frac{y(x_{i+1})-y(x_i)}{\Delta x} = y'(x_i)+\frac{1}{2}y''(x_i)\Delta x+\ldots, \tag{4.2}$$

where the error $(1/2)y''(x_i)\Delta x$ is to first order in Δx, i.e., $O(\Delta x)$.

2. Backward differences:

$$\left.\frac{dy}{dx}\right|_{x_i} \approx \frac{y_i-y_{i-1}}{\Delta x}. \tag{4.3}$$

Then

$$\begin{aligned} y(x_i)-y(x_{i-1}) &= y(x_i)-\left[y(x_i)-y'(x_i)\Delta x+\frac{1}{2}y''(x_i)\Delta x^2-\ldots\right], \\ \frac{y(x_i)-y(x_{i-1})}{\Delta x} &= y'(x_i)-\frac{1}{2}y''(x_i)\Delta x+\ldots, \end{aligned} \tag{4.4}$$

so the error is again to first order in Δx.

3. Centered differences:

$$\left.\frac{dy}{dx}\right|_{x_i} \approx \frac{y_{i+1}-y_{i-1}}{2\Delta x}. \tag{4.5}$$

Then

$$\begin{aligned} y(x_{i+1})-y(x_{i-1}) &= y(x_i)+y'(x_i)\Delta x+\frac{1}{2}y''(x_i)(\Delta x)^2+\frac{1}{6}y'''(x_i)(\Delta x)^3\ldots \\ &\quad -\Big[y(x_i)-y'(x_i)\Delta x+\frac{1}{2}y''(x_i)(\Delta x)^2 \\ &\quad -\frac{1}{6}y'''(x_i)(\Delta x)^3+\ldots\Big], \end{aligned} \tag{4.6}$$

$$\begin{aligned} &= 2y'(x_i)\Delta x+\frac{2}{6}y'''(x_i)(\Delta x)^3+\ldots, \\ \frac{y(x_{i+1})-y(x_{i-1})}{2\Delta x} &= y'(x_i)+\frac{1}{6}y'''(x_i)(\Delta x)^2+\ldots. \end{aligned} \tag{4.7}$$

Then the error of this approximation is to second order in Δx, i.e., $O((\Delta x)^2)$. We see that the centered difference is a good approximation and is more accurate than the other two.

We continue examining finite differences by finding the estimation of the second order derivative, which can be found by the approximation

$$\left.\frac{d^2y}{dx^2}\right|_{x_i} \approx \frac{y_{i+1} - 2y_i + y_{i-1}}{(\Delta x)^2},$$

which has an error of $O((\Delta x)^2)$.

The finite difference method can be applied to a simple parabolic partial differential equation, such as the diffusion equation,

$$\frac{\partial f}{\partial t} = -\frac{\partial S}{\partial x}, \tag{4.8}$$

where f is a particle density and

$$S = -D\frac{\partial f}{\partial x}.$$

We approximate f by setting $f_i^n \approx f(t_n, x_i)$. We want to find f_i^{n+1} for $i = 1, \ldots, N-1$, and after that find f_i^{n+2}, f_i^{n+3}, ... Therefore, when we apply the finite difference method, we will get

$$\begin{aligned}\frac{f_i^{n+1} - f_i^n}{\Delta t} &= \frac{S\left(x_i - \frac{\Delta x}{2}\right) - S\left(x_i + \frac{\Delta x}{2}\right)}{\Delta x}, \\ &= \frac{-D\left(x - \frac{\Delta x}{2}\right)\frac{f_i - f_{i-1}}{\Delta x} + D\left(x + \frac{\Delta x}{2}\right)\frac{f_{i+1} - f_i}{\Delta x}}{\Delta x},\end{aligned} \tag{4.9}$$

and if D is constant in x, we have

$$\frac{f_i^{n+1} - f_i^n}{\Delta t} = \frac{D}{(\Delta x)^2}\left[f_{i-1} - 2f_i + f_{+1}\right]. \tag{4.10}$$

Given an initial condition for f_i^0, we now have the equation to solve the distribution function at every time.

There are various methods for applying finite differencing to solve parabolic partial differential equations.

Explicit Method: This method is related to forward differencing in t. From equation (4.10), in this case the bracketed term is evaluated at time t_n:

$$\frac{f_i^{n+1} - f_i^n}{\Delta t} = \frac{D}{(\Delta x)^2}\left[f_{i-1}^n - 2f_i^n + f_{i+1}^n\right], \tag{4.11}$$

$$f_i^{n+1} = f_i^n + \frac{D\Delta t}{(\Delta x)^2}\left[f_{i-1}^n - 2f_i^n + f_{i+1}^n\right]. \tag{4.12}$$

The error of this method is $a\Delta t + b((\Delta x)^2)$ to leading order, for some constants a, b. An unstable result will be obtained if $\Delta t > (\Delta x)^2/2D$.

Implicit Method: This method is related to backward differencing. Evaluating the bracketed term at t_{n+1}, we get

$$\frac{f_i^{n+1} - f_i^n}{\Delta t} = \frac{D}{(\Delta x)^2}\left[f_{i-1}^{n+1} - 2f_i^{n+1} + f_{i+1}^{n+1}\right], \tag{4.13}$$

$$f_i^{n+1} - \frac{D\Delta t}{(\Delta x)^2}\left[f_{i-1}^{n+1} - 2f_i^{n+1} + f_{i+1}^{n+1}\right] = f_i^n. \tag{4.14}$$

We have to solve a matrix equation because our equations are coupled, linear equations. Then this method is harder to program than the explicit method but the results are more stable. The error of this method is still $a\Delta t + b((\Delta x)^2)$.

The combination between explicit and implicit methods can reduce the error from $O(\Delta t)$ to $O(\Delta t^2)$. The combination is called the Crank-Nicolson method.

Crank-Nicolson Method:

Crank-Nicolson method $\longleftarrow$ $\frac{1}{2}$explicit method+$\frac{1}{2}$implicit method

The relation between f^{n+1} and f^n is

$$\frac{f_i^{n+1} - f_i^n}{\Delta t} = \frac{D}{(\Delta x)^2}\left\{\frac{f_{i-1}^n - 2f_i^n + f_{i+1}^n}{2} + \frac{f_{i-1}^{n+1} - 2f_i^{n+1} + f_{i+1}^{n+1}}{2}\right\}, \tag{4.15}$$

$$f_i^{n+1} = f_i^n + \frac{D\Delta t}{2(\Delta x)^2}\left\{f_{i-1}^n - 2f_i^n + f_{i+1}^n + f_{i-1}^{n+1} - 2f_i^{n+1} + f_{i+1}^{n+1}\right\}. \quad (4.16)$$

If we set $r = D\Delta t/2(\Delta x)^2$, then equation (4.16) becomes

$$-rf_{i-1}^{n+1} + (1+2r)f_i^{n+1} - rf_{i+1}^{n+1} = rf_{i-1}^n + (1-2r)f_i^n + rf_{i+1}^n. \quad (4.17)$$

This is again a coupled set of linear equations, with one equation per i value of interest. This can be arranged in the form of a matrix equation. If we solve the matrix equation, we will find the distribution function that we want.

4.1.2 TVD

The Total Variation Diminishing (TVD) method can be used to solve the streaming-convection part of the transport equation. The TVD algorithm used by Hatzky (1996) showed a faster running speed than the method used by Ruffolo (1995). Another advantage of TVD is limiting the amount of numerical diffusion. Motivated by the results of Hatzky, the algorithm of Roe (1985) was adjusted to allow a general Courant number, $\gamma = v_z\Delta t/\Delta z$, so our simulations can use a general value of Δz (Nutaro et al. 2001).

The TVD method was first described by Harten (1983) for an oscillation-free scheme. The total variation of a function $F(x)$ is defined by

$$TV(F) = \int \left|\frac{\partial F}{\partial x}\right| dx, \quad (4.18)$$

and this expression has a numerical (finite difference) form of

$$TV\left(F^n\right) = \sum_l \left|F_{l+1}^n - F_l^n\right|, \quad (4.19)$$

where l is the spatial index and n is the time index. The essential requirement of this method is

$$TV\left(F^{n+1}\right) \leq TV\left(F^n\right), \quad (4.20)$$

in which case this method is called total variation diminishing (TVD). The TVD method gives the possibility of more accurate and oscillation-free solutions. However, a typical implementation of this method limits the Courant number to $0 \leq \gamma \leq 1$. An application by Nutaro et al. makes the method able to use a general value of γ, which means we can use various Δz. We first consider the case where v_z does not depend on z. Using the TVD method, F is moved by an integral number of steps, g, received from rounding γ downward. As an example, when $\gamma = 2.6$, F is moved forward by 2 z-grid points, so that $g = 2$ and the remainder is equal to 0.6. We call the remainder γ', which is between 0 and 1. We are interested in the distribution function at a grid point l, F_l. We get this value from

$$F_l \leftarrow F_{l-g} - \frac{\Delta t}{\Delta z} S'_{l+\frac{1}{2}} + \frac{\Delta t}{\Delta z} S'_{l-\frac{1}{2}}, \tag{4.21}$$

where $S'_{l+\frac{1}{2}}$ is the flux from l to $l+1$, which depends on γ'. We can find the flux from

$$S'_{l+\frac{1}{2}} = v'_{l+\frac{1}{2}} F_{l-g} + \frac{1}{2} v'_{l+\frac{1}{2}} (1 - \gamma'_{l+\frac{1}{2}})(F_{l-g+1} - F_{l-g})\varphi_{l-g}, \tag{4.22}$$

where $v'_{l-\frac{1}{2}}$ is $\gamma'_{l-\frac{1}{2}} \Delta z / \Delta t$ at $z = z_l - \Delta z/2$, and φ_l is the flux limiter (Roe 1985).

If we consider v_z dependent on z, then γ changes in z, and the distribution function at l is set to

$$F_l \leftarrow \left(\sum_{m=l-g_-}^{l-g_+} F_m \right) - \frac{\Delta t}{\Delta z} \left(S'_{l+\frac{1}{2}} - S'_{l-\frac{1}{2}} \right), \tag{4.23}$$

where $g_+(g_-)$ are rounded-down integers corresponding to $\gamma_{l+1/2}(\gamma_{l-1/2})$. The formula in equation (4.23) is constrained so that $g_+ \leq g_- + 1$; sometimes this constraint can be avoided by choosing small Δt. If $g_+ = g_- + 1$ the sum will be zero.

4.1.3 Interpolation

An interpolation method is used to estimate an unknown value from neighboring values that are known. Now we present the linear interpolation method in one dimension (see Figure 4.1). We have a function $F(x)$ which varies in one dimension, x. If we know the values of the function at points x_i and x_{i+1}, we can

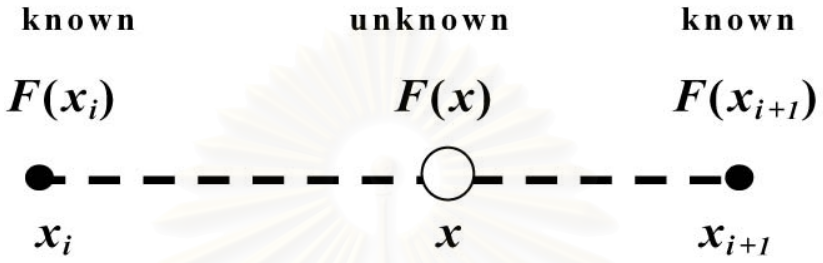

Figure 4.1: Linear interpolation in one dimension. The black circles are the points where we know the values of F, while the white circle is the point where we want to find the value of F.

estimate the value at point x by the relation:

$$F(x) = \frac{x_{i+1} - x}{x_{i+1} - x_i} F(x_i) + \frac{x - x_i}{x_{i+1} - x_i} F(x_{i+1}). \tag{4.24}$$

We can define

$$f_x = \frac{x - x_i}{x_{i+1} - x_i}, \tag{4.25}$$

where f_x is the fractional distance of x from x_i to x_{i+1}. It has a value between 0 and 1 for interpolation, and for extrapolation, $f_x < 0$ or $f_x > 1$. Equation (4.24) becomes

$$F(x) = (1 - f_x)F(x_i) + f_x F(x_{i+1}). \tag{4.26}$$

We use such an interpolation method to solve for the p-transport of distribution function. The only part of acceleration of the transport equation (where

$\partial \vec{U}/\partial t$ is zero in our work) is

$$\frac{\partial F(t,z,\mu,p)}{\partial t} = -\frac{\partial}{\partial p} p \left[\frac{1-3\mu^2}{2} l_i l_j \frac{\partial U_j}{\partial x_i} - \frac{1-\mu^2}{2} \vec{\nabla} \cdot \vec{U} \right] F(t,z,\mu,p). \tag{4.27}$$

Referring to equation (3.6), the term in brackets can be interpreted as $(1/p)\Delta p/\Delta t$. Setting this to the inverse of a characteristic acceleration time, τ_a, we have

$$\frac{1}{\tau_a} = \frac{1-3\mu^2}{2} l_i l_j \frac{\partial U_j}{\partial x_i} - \frac{1-\mu^2}{2} \vec{\nabla} \cdot \vec{U}, \tag{4.28}$$

which is constant in p, and equation (4.27) becomes

$$\frac{\partial}{\partial t} F(t,z,\mu,p) = -\frac{1}{\tau_a} \frac{\partial}{\partial p} pF(t,z,\mu,p). \tag{4.29}$$

Another form is

$$\frac{\partial}{\partial t} pF(t,z,\mu,p) = -\frac{1}{\tau_a} \frac{\partial}{\partial \ln(p/p_0)} pF(t,z,\mu,p), \tag{4.30}$$

where p_0 is a fixed reference momentum, which has the solution in the form of

$$pF(t+\Delta t,z,\mu,p) = pe^{-\Delta t/\tau_a} F(t,z,\mu,pe^{-\Delta t/\tau_a}). \tag{4.31}$$

In other words, from equation (4.30), the value of pF is constant along characteristics, which are straight lines of slope $1/\tau_a$ in the graph of $\ln p$ versus t (see Figure 4.2).

Referring to Figure 4.2, the value of $F(t_{i+1}, p_w)$ can be found from $F(t_i, p^*)$. The point p^* is defined by the relation

$$\frac{dp}{dt} = \frac{p}{\tau_a}, \tag{4.32}$$

$$p^* = p_w e^{-\Delta t/\tau_a}. \tag{4.33}$$

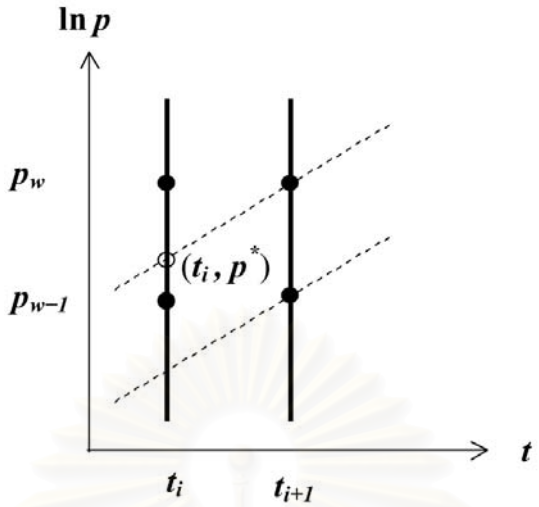

Figure 4.2: The interpolation scheme. The solid lines are at constant t. The dashes lines are characteristics, along which pF is constant. The value of $F(t_{i+1}, p_w)$ can be found from $F(t_i, p^*)$, which can be estimated by interpolation between $F(t_i, p_{w-1})$ and $F(t_i, p_w)$.

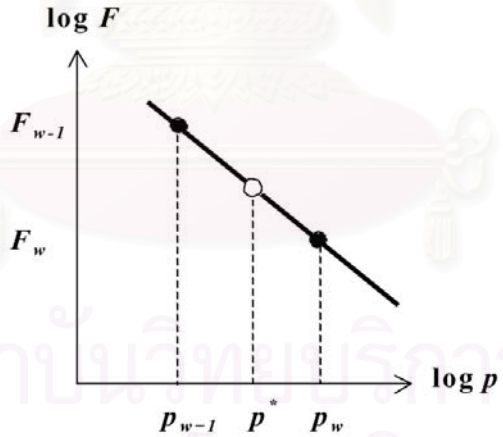

Figure 4.3: The geometric interpolation between F_{w-1} and F_w at constant t to estimate $F(p^*)$.

We use geometric interpolation, which is linear interpolation in a log-log plot (see Figure 4.3). The value at point p^* can be estimated by geometric interpolation between $F_{w-1} = F(p_{w-1})$ and $F_w = F(p_w)$ at constant t. The value of $F(p^*)$ can be found by the relation

$$\log F(p^*) = (1 - f_p) \log F_{w-1} + f_p \log F_w, \tag{4.34}$$

where

$$f_p = \frac{\log p^* - \log p_{w-1}}{\log p_w - \log p_{w-1}}. \tag{4.35}$$

Substituting equation (4.35) into equation (4.34), the result is

$$\log F(p^*) = \log F_{w-1} + \frac{\log F_{w-1} - \log F_w}{\log p_{w-1} - \log p_w}(\log p^* - \log p_{w-1}). \tag{4.36}$$

If we set

$$expon = \frac{\log F_{w-1} - \log F_w}{\log p_{w-1} - \log p_w}, \tag{4.37}$$

the equation (4.36) becomes

$$p^* F(p^*) = p_{w-1} F_{w-1} \left(\frac{p^*}{p_{w-1}} \right)^{expon+1}, \tag{4.38}$$

Then $p_w F(t + \Delta t, \mu, z, p_w)$ is set equal to $p^* F(t, p^*)$. The numerical simulation in this part (for deceleration or acceleration) is performed in the code decel.c, shown in Appendix A.

4.1.4 Solving the Diffusion-Convection Equation

The diffusion-convection equation (3.66) is solved by a shooting method. This equation is divided into two 1^{st}- order differential equations, for F and S. The boundary conditions are $F = 1$ and the flux S equal to the fluid speed far downstream, and S far upstream equal to zero. The details of this solution are demonstrated in Kanin Aungskulsiri's senior project.

4.2 Test for a Single Step and Finding Appropriate Step Sizes

It is difficult to solve the transport equation in one step. Therefore, we employ the operator splitting method (Park and Petrosian 1996; Press et al. 1992, Chap. 19). The right hand side of the transport equation (3.7) is separated into three components, which depend on each of the operators ($\partial/\partial\mu$, $\partial/\partial z$, $\partial/\partial p$). The distribution function, $F(t, \mu, z, p)$ is updated in the following steps:

1. Updates F for μ-changing processes over a time $\Delta t/2$.
2. Updates F for p-changing processes over a time Δt.
3. Updates F for z-changing processes over a time Δt.
4. Updates F for μ-changing processes over a time $\Delta t/2$.

Since the error of the simulation depends on the step sizes of the variables, then one way to measure the accuracy of the simulation is testing for a single step in time, Δt. We do this by comparison of results between the operator splitting method and the emuz.c program for the special case of $F(t = 0, \mu, z, p) \equiv 1$, which is our initial condition, and for which we can readily calculate $\partial F/\partial t$ from equation (3.8). The program emuz.c (Kanokporn Leerungnavarat's work, see Appendix B) is used for calculating each component of $(1/F)\partial F/\partial t$, which are the streaming-convection, scattering-focusing, and acceleration terms at one time step, Δt. The emuz.c program considers each momentum value and varies z from $-16*zstep$ to $16*zstep$, μ from $-1*mustep$ to $1*mustep$, where $zstep$ and $mustep$ are the step sizes of the simulation in z and μ, respectively. (Note that z=0 at the center of the compression, and μ is the pitch angle cosine so it varies from -1 to +1.) The summation of the results from each component gives the distribution function after one time step, $F(\Delta t, \mu, z, p)$. These values are compared with the

results for each component from the transport code, using the operator splitting method over one time step.

The change in the distribution function is indicated by shading in the contour plots of μ and z (see Figures 4.4-4.5), which show the results from $v/U_{1n} = 10$ and $v/U_{1n} = 50$, respectively). Each Figure has two panels. The top panel shows the results from the emuz.c program, while the bottom panel shows the results from the hybwind.diag.c program. Both of them have a roughly circular structure and similar shading. The inner shade indicates maximum F, while expanding to the outer shade, F approaches 1. The maximum F occurs from the acceleration at the center of the compression. The accelerated particles accumulate as shown by the high F. A similar shading pattern in the two panels indicates acceptable step sizes, Δz, Δt, and $\Delta \mu$. In practice, we vary those values, and look at the shading and structure, comparing the values of F from emuz.c and the transport code for a single step. We want large step sizes for decreasing the run time, but those values should not cause an unacceptable error. We have also performed complete simulations for different step sizes to confirm the accuracy of the simulations.

4.3 Simulation Procedure

The purposes of our simulations are to find the steady-state spectral index (a parameter to describe the particle acceleration), which is related to $F \propto p^{-\gamma}$, and to find the relation between F and z at various compression widths. There are six cases of running that depend on the particle momentum and the compression width divided by the scattering mean free path. The procedure of running, shown in Figure 4.6, is as follows:

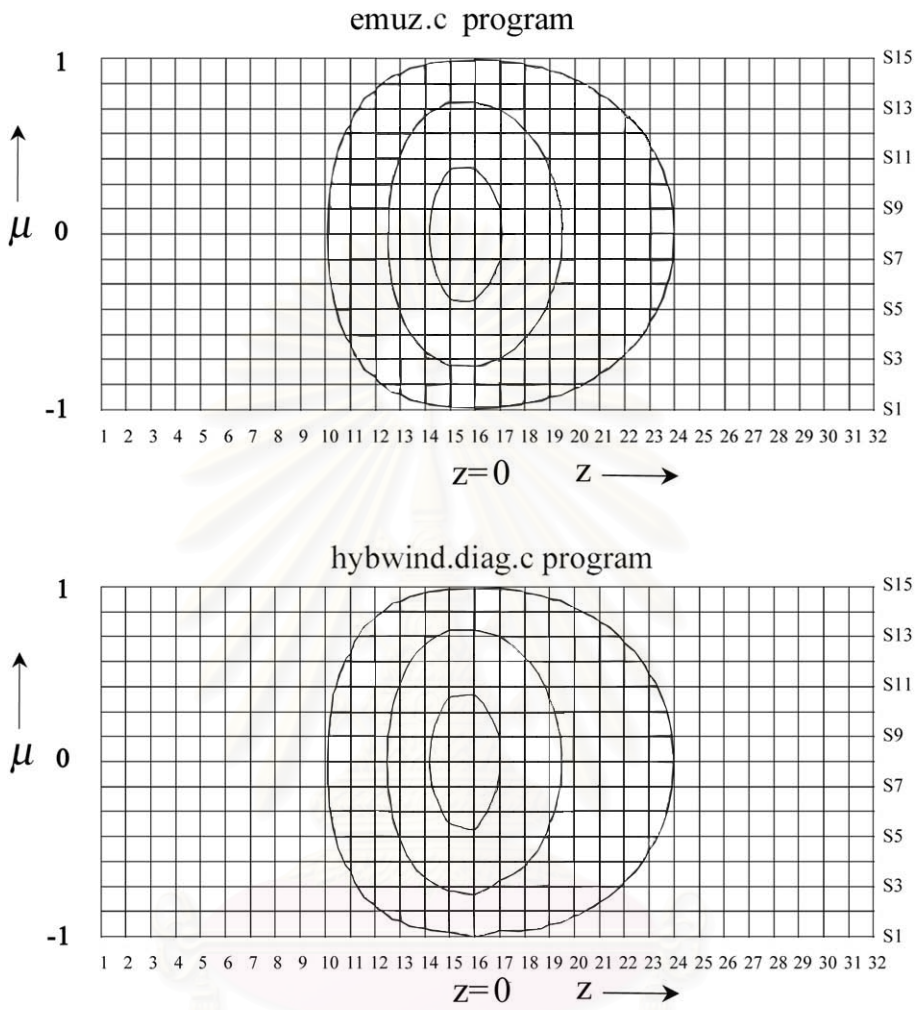

Figure 4.4: The contour plot of ΔF for $v/U_{1n} = 10, b/\lambda = 0.2$, and the initial condition $F(\mu, z) \equiv 1$. The step sizes are $\Delta z = 0.03125$ AU, $\Delta\mu = 2/15$, and $\Delta t = 2.86325$ minutes ($v\Delta t = 0.03125$ AU). Contours indicate $\Delta F = 0.0125$, 0.0075, and 0.0025 from the inside to the outside. Top panel: approximate analytic solution. Bottom panel: numerical solution.

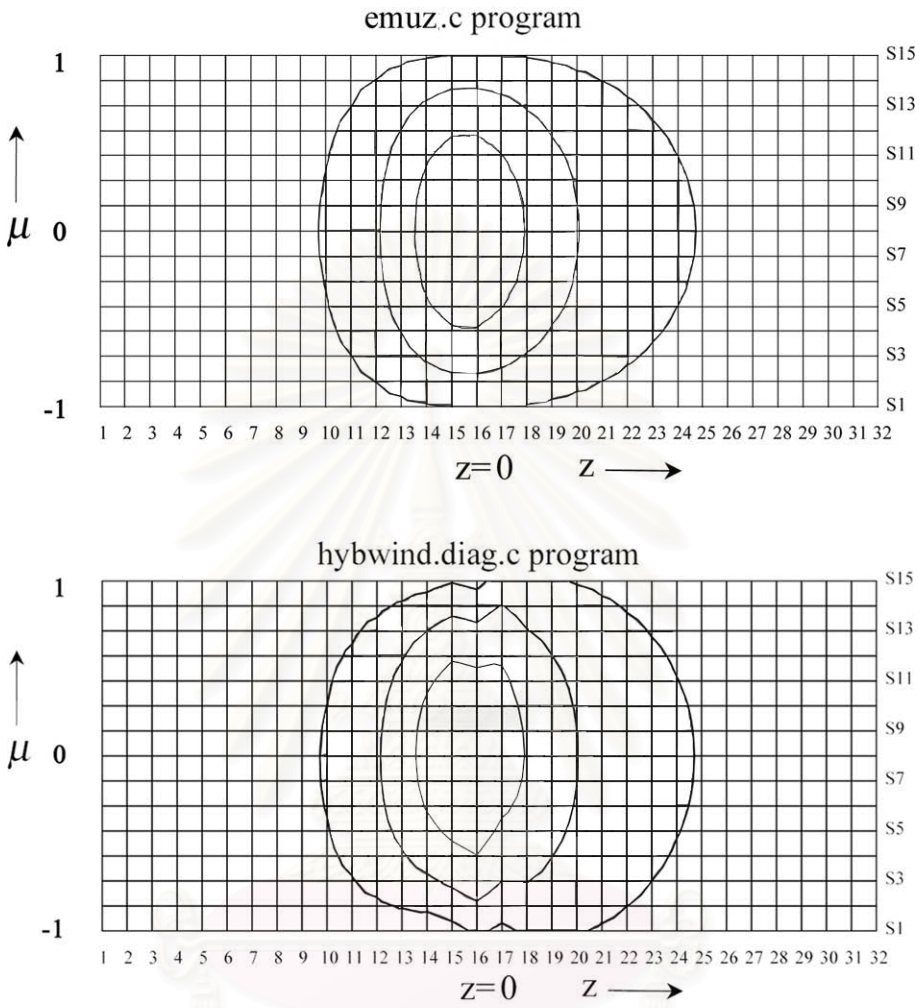

Figure 4.5: The contour plot of ΔF for $v/U_{1n} = 50, b/\lambda = 0.2$, and the initial condition $F(\mu, z) \equiv 1$. The step sizes are $\Delta z = 0.00625$ AU, $\Delta\mu = 2/15$, and $\Delta t = 0.6239625$ minutes ($v\Delta t = 0.00625$ AU). Contours indicate $\Delta F = 0.0025$, 0.0015, and 0.0005 from the inside to the outside. Top panel: approximate analytic solution. Bottom panel: numerical solution.

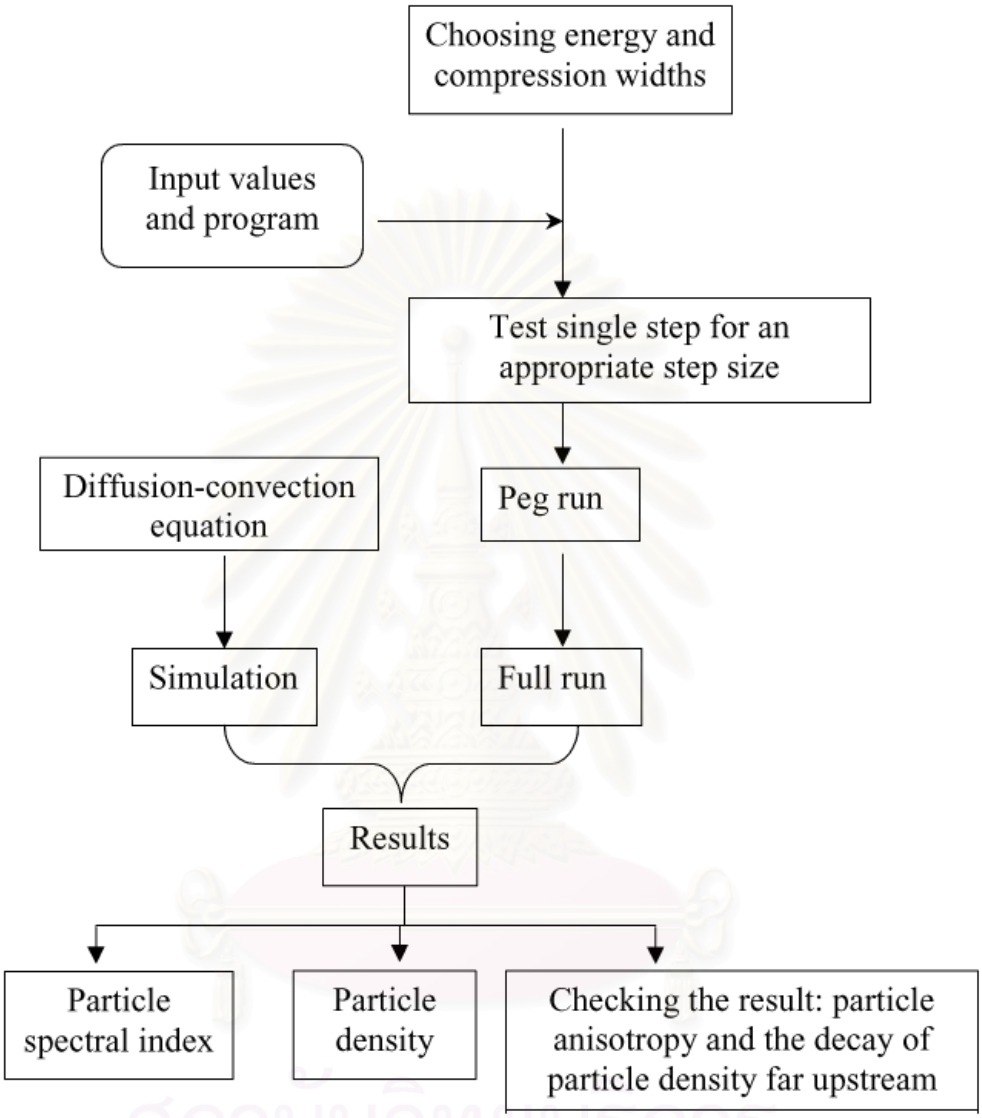

Figure 4.6: The procedure of running.

1. Choosing v/U_{1n} that we are interested in. This value is related to the particle momentum.

2. Choosing Δz, Δt, and $\Delta \mu$.

3. Testing the accuracy of the distribution function in one time step, which depends on Δz, Δt, and $\Delta \mu$.

4. Peg run: for estimating the initial value for the distribution function at low momentum (used as a "peg" or p-boundary condition in the full run).

5. Full run: for finding the steady-state best gamma at different energies and compression widths, for finding the distribution function versus z, and for testing the accuracy of the transport equation program.

6. Finding the error of gamma, checking the steady-state running, and understanding all values from running.

7. Running with other compression widths.

4.4 Simulation Program and Inputs

The program that we use to perform simulations is composed of 9 files:

1. hybwind.c: It is the main program, all functions and initial values are called from here.

2. decel.c: It is used to calculate the deceleration or acceleration term.

3. field.c: The magnetic structure is defined in this routine.

4. initial.c: It sets the initial value of F.

5. inject.c: It is used to describe the injection of particles during the simulation (not used in this work).

6. nrutil.c: It reserves memory for arrays used in the program.

7. printout.c: The results are printed out here.

8. stream.c: It is used to calculate the effects of the streaming and convection.

9. tridag.c: It is used to solve a tridiagonal matrix equation (from Press et al. 1988).

The advantage of separating files is that we can develop this program for many physical problems by changing only certain files. This is called a modular approach. The input values of the simulation are:

1. start time (minutes),
2. stop time (minutes),
3. time step (minutes),
4. print time (minutes),
5. number of μ grid points,
6. number of p grid points,
7. momentum values (MeV/c),
8. length in the z direction (AU),
9. step size in z (AU),
10. particle mass (MeV/c^2),
11. solar wind speed divided by c,
12. parallel scattering mean free path (AU),
13. scattering power law index,
14. whether to print extra diagnostic information.

For choosing the previous input values, 1-14, we conveniently set the start time to be zero and we set the stop time to be sufficient for the simulation to approach close to a steady-state. We select the time step from single step testing.

The print time is set to the time step for frequent printing of results. The number of μ grid points is usually used as 15, but it can also be increased for checking the accuracy. The p-grid points usually follow the momentum values of interest. In this work we use 5 momentum values. The momentum values are related to v/U_{1n}. The length is set to 1 AU in the z direction, where λ is set to 1 AU. In other words, the z range is 1 in units of λ (or 0.5 on either side of the shock or compression). The value of the scattering power law index is set to 1.0, which means that the scattering is isotropic (a standard assumption). We do not want to print extra diagnostic information, so this value is set to zero.

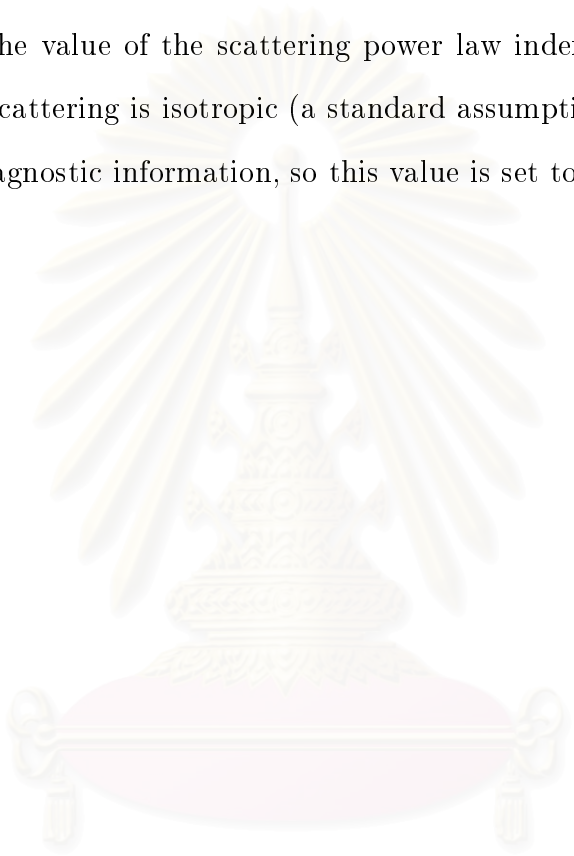

Chapter 5
Results and Discussion

5.1 Results

In this work we are interested in the acceleration of cosmic ray particles to $v/U_{1n} = 50$ (or for protons, a kinetic energy E of 3.891 MeV), where v is the particle velocity and U_{1n} is the upstream solar wind velocity normal to the compression region, and also to a lower energy with $v/U_{1n} = 10$ ($E = 0.155$ MeV). For each momentum (energy) value we simulate for three cases of the width of the compression region, that is, $b/\lambda_{||} = 0.2$, $b/\lambda_{||} = 0.5$, and $b/\lambda_{||} = 1.0$. Thus we present results for six cases. The other constant values that we use for these results are:

- the proton mass, m=938.27 MeV/c^2,
- the solar wind speed divided by the speed of light far upstream, $U_{1n}/c = 0.001816$,
- the scattering mean free path, $\lambda_{||} = 1.0$ AU,
- the angle between the magnetic field line and compression normal far upstream, $\theta_1 = \tan^{-1}(4.0)$,
- the angle between the magnetic field line and compression normal far downstream, $\theta_2 = \tan^{-1}(15.11)$,

5.1.1 Distribution Function

From the simulations we get results about the acceleration of particles in terms of the distribution function of particles averaged over pitch angle, $\langle F \rangle_\mu$. From the distribution function, we can derive the density of cosmic ray particles that can be accelerated to the momentum of interest by the whole process that we discussed in Chapter 3. We normalize this value to the particle density far downstream. For a shock one can observe a peak in the particle density just upstream of the shock (Ruffolo 1999, Gieseler et al. 1999). In this work, we observe a similar peak for the narrower compressions. We identify this type of peak as a "mirroring peak," which comes from the magnetic mirroring (reflection) of particles when they encounter the compression region.

The distribution function vs. the distance z normal to the shock or compression plane in each case is shown in Figures 5.1 - 5.4. Here we consider both the case of a shock (Figure 5.1) and compressions of varying widths for different particle speeds (Figures 5.2 - 5.7).

5.1.2 Spectral Index

The next set of results involves the spectral index of accelerated particles, γ. We can use the spectral index to describe the efficiency of acceleration because the results from cosmic ray observations and existing theory have shown that the relation between $\langle F \rangle_\mu$ and the particle momentum, p, ought to be a power law, $\langle F \rangle_\mu \propto p^{-\gamma}$. Also γ is a key measurable quantity and is important in determining whether a model of acceleration at compressions can explain measured data, as suggested by Jokipii et al. (2001). Thus we find the spectral index in the steady state. Simulation results are displayed in Figures 5.8 - 5.14. These figures display

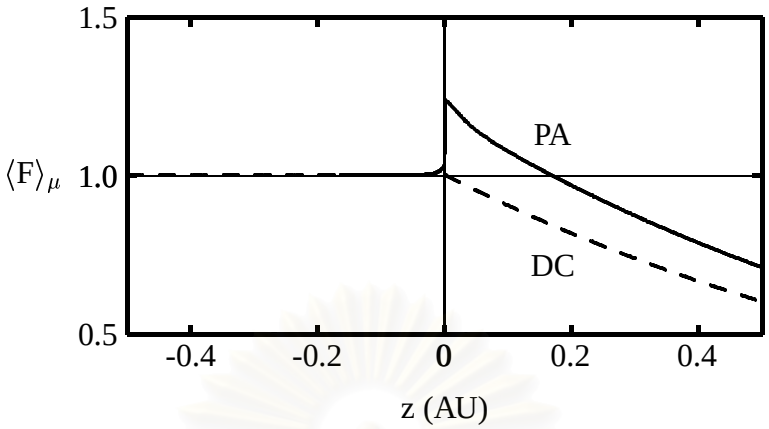

Figure 5.1: Distribution function averaged over pitch angle cosine vs. the distance z at $v/U_{1n} = 50$, for a shock ($b/\lambda_{\|} = 0$). PA: pitch-angle transport equation, DC: diffusion-convection equation.

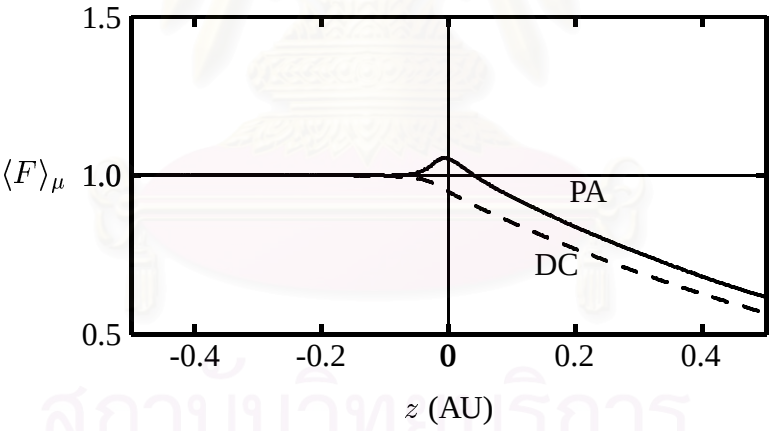

Figure 5.2: Distribution function averaged over pitch angle cosine vs. the distance z at $v/U_{1n} = 50$, $b/\lambda_{\|} = 0.2$. PA: pitch-angle transport equation, DC: diffusion-convection equation.

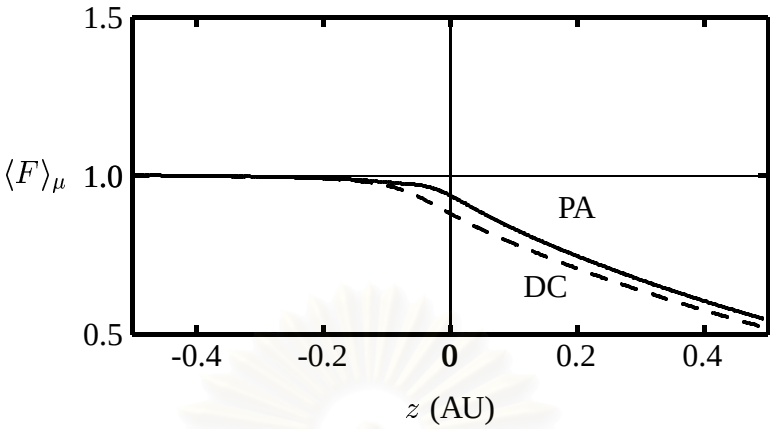

Figure 5.3: Distribution function averaged over pitch angle cosine vs. the distance z at $v/U_{1n} = 50$, $b/\lambda_{\|} = 0.5$. PA: pitch-angle transport equation, DC: diffusion-convection equation.

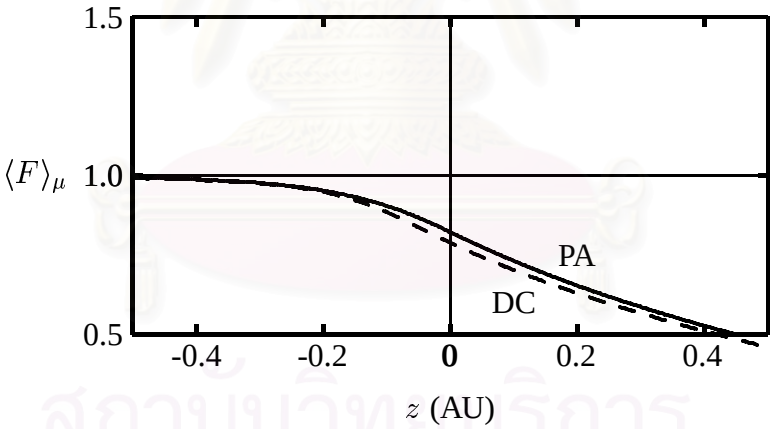

Figure 5.4: Distribution function averaged over pitch angle cosine vs. the distance z at $v/U_{1n} = 50$, $b/\lambda_{\|} = 1.0$. PA: pitch-angle transport equation, DC: diffusion-convection equation.

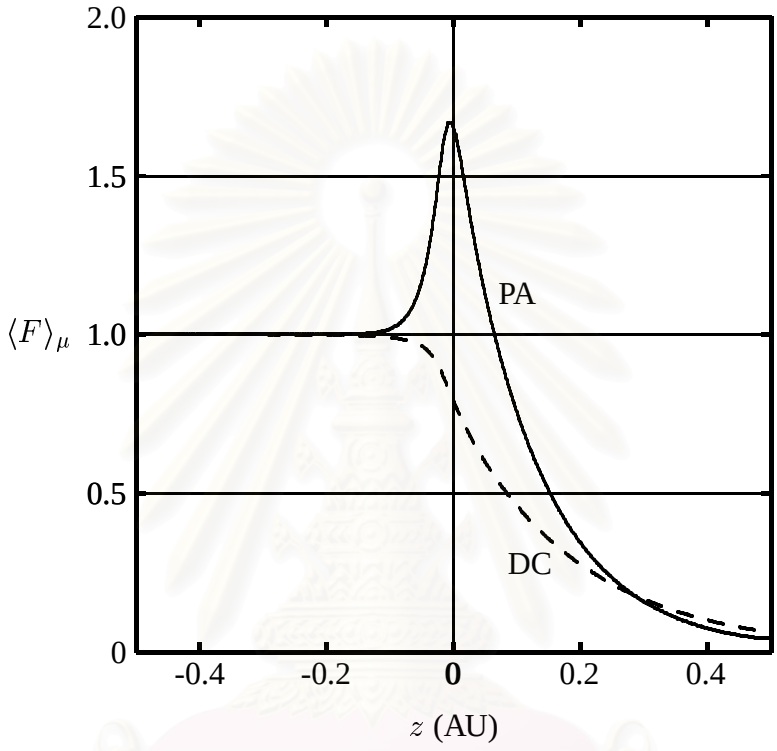

Figure 5.5: Distribution function averaged over pitch angle cosine vs. the distance z at $v/U_{1n} = 10$, $b/\lambda_{\|} = 0.2$. PA: pitch-angle transport equation, DC: diffusion-convection equation.

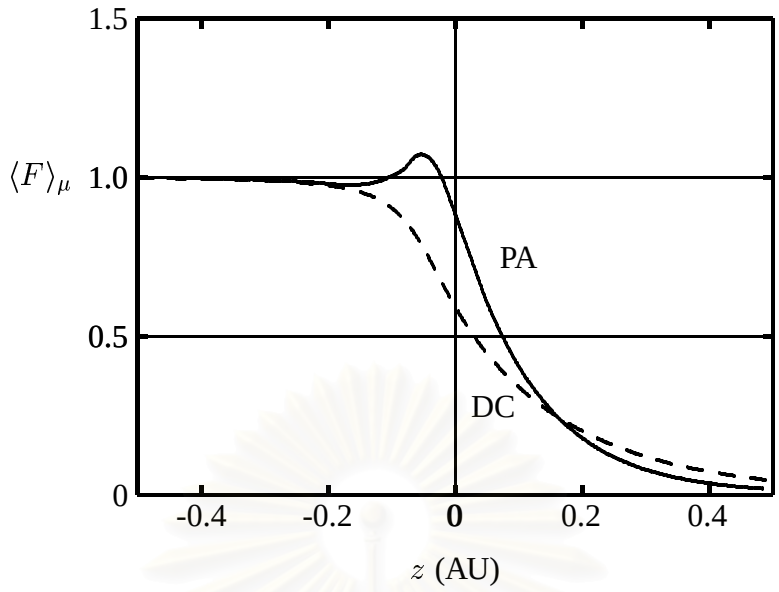

Figure 5.6: Distribution function averaged over pitch angle cosine vs. the distance z at $v/U_{1n} = 10$, $b/\lambda_{\|} = 0.5$. PA: pitch-angle transport equation, DC: diffusion-convection equation.

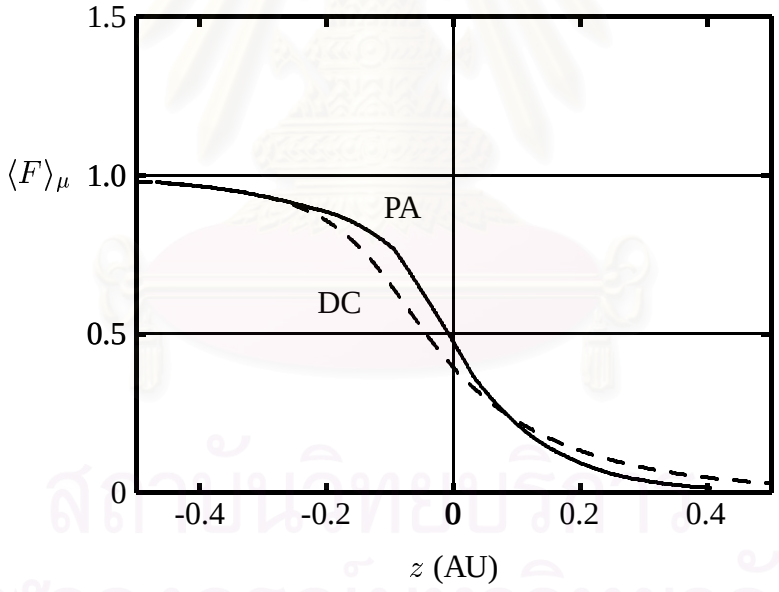

Figure 5.7: Distribution function averaged over pitch angle cosine vs. the distance z at $v/U_{1n} = 10$, $b/\lambda_{\|} = 1.0$. PA: pitch-angle transport equation, DC: diffusion-convection equation.

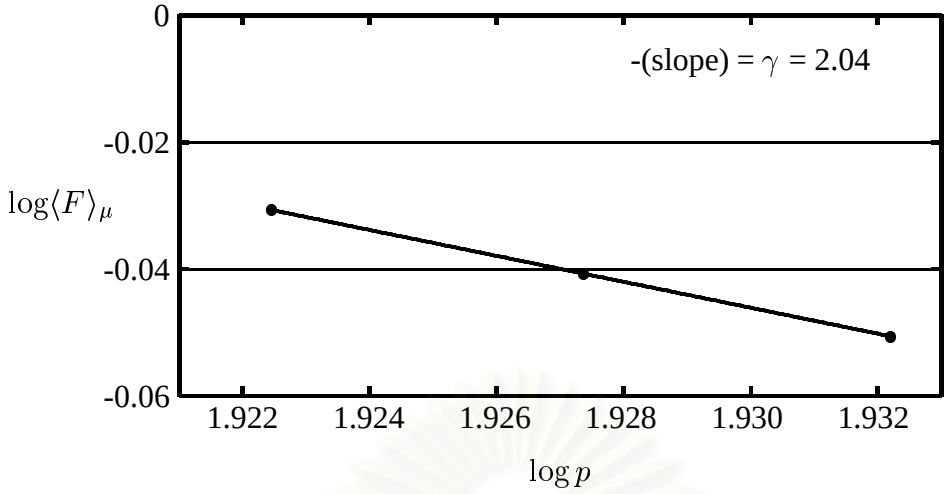

Figure 5.8: Downstream $\log\langle F\rangle_\mu$ vs. $\log p$ at $v/U_{1n} = 50$, for a shock ($b/\lambda_{\|} = 0$).

the relation between $\log\langle F\rangle_\mu$ (far downstream) and $\log p$, where p is in units of MeV/c. Since γ depends on the momentum p, we evaluate γ by plotting points (bullets) for the simulation results at momentum values closest to the momentum of interest, and the line represents the best-fit straight line. The slope of this line is our determination of $-\gamma$. The results of the spectral index vs. compression width for two values of the ratio v/U_{1n} are shown in Figure 5.15.

5.1.3 Anisotropy

As explained in §3.4 (and using $l_z = \cos\theta$, where θ is the angle between the magnetic field line and the particle momentum), the anisotropy of the particle distribution, δ, is expected to be $-3U_{1n}/(v\cos\theta) + U_{1n}v\cos\theta/c^2$ far upstream and $U_{1n}v\cos\theta/c^2$ far downstream. However, in this work we use U much less than c, so the value of δ far downstream is expected to be close to zero. The anisotropy vs. z is shown in Figures 5.16 - 5.21. The arrows point to the constant value far upstream that is expected from equation (3.77).

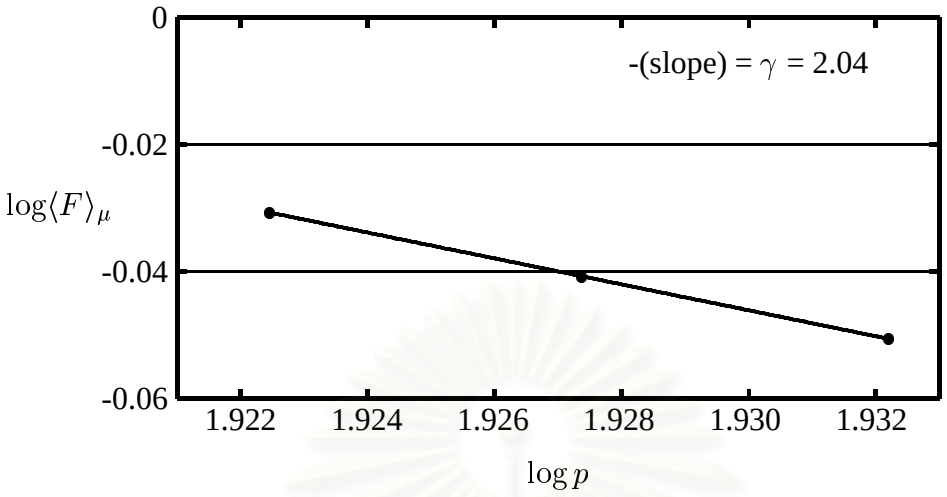

Figure 5.9: Downstream $\log\langle F\rangle_\mu$ vs. $\log p$ at $v/U_{1n} = 50$, $b/\lambda_{||} = 0.2$.

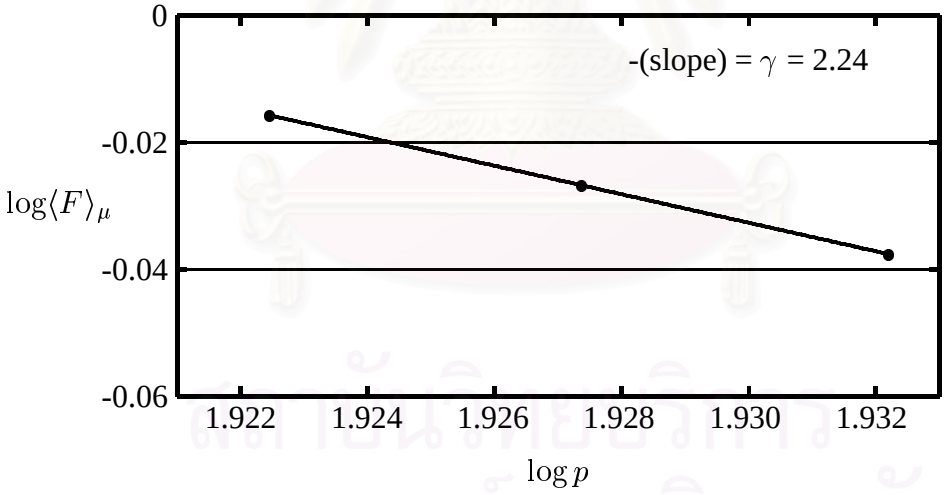

Figure 5.10: Downstream $\log\langle F\rangle_\mu$ vs. $\log p$ at $v/U_{1n} = 50$, $b/\lambda_{||} = 0.5$.

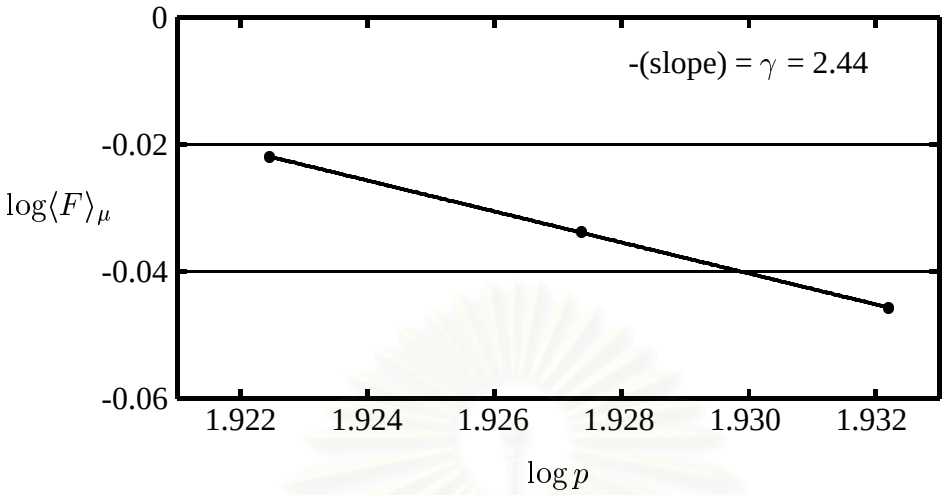

Figure 5.11: Downstream $\log\langle F\rangle_\mu$ vs. $\log p$ at $v/U_{1n} = 50$, $b/\lambda_{\|} = 1.0$.

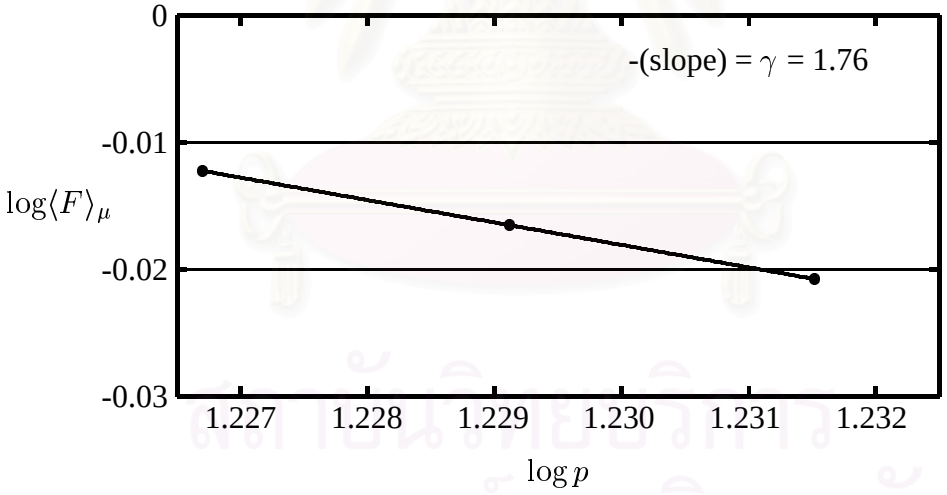

Figure 5.12: Downstream $\log\langle F\rangle_\mu$ vs. log at $v/U_{1n} = 10$, $b/\lambda_{\|} = 0.2$.

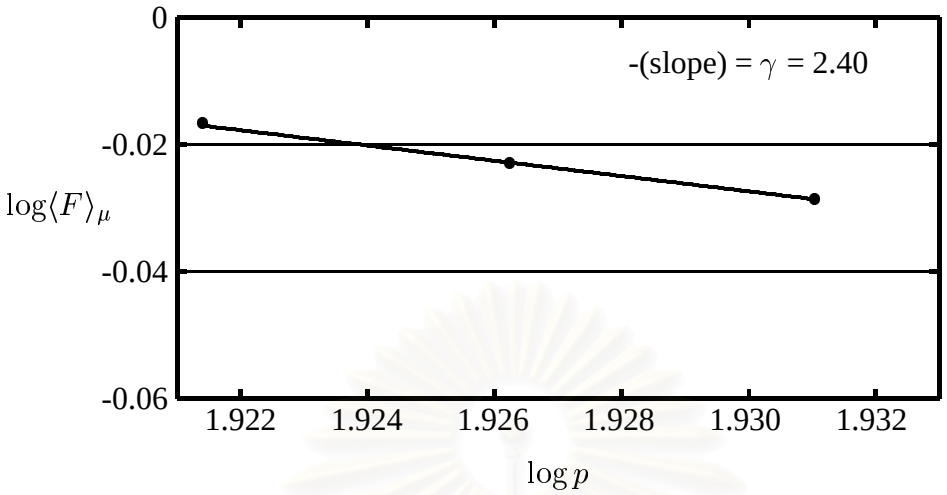

Figure 5.13: Downstream $\log\langle F\rangle_\mu$ vs. log at $v/U_{1n} = 10$, $b/\lambda_{||} = 0.5$.

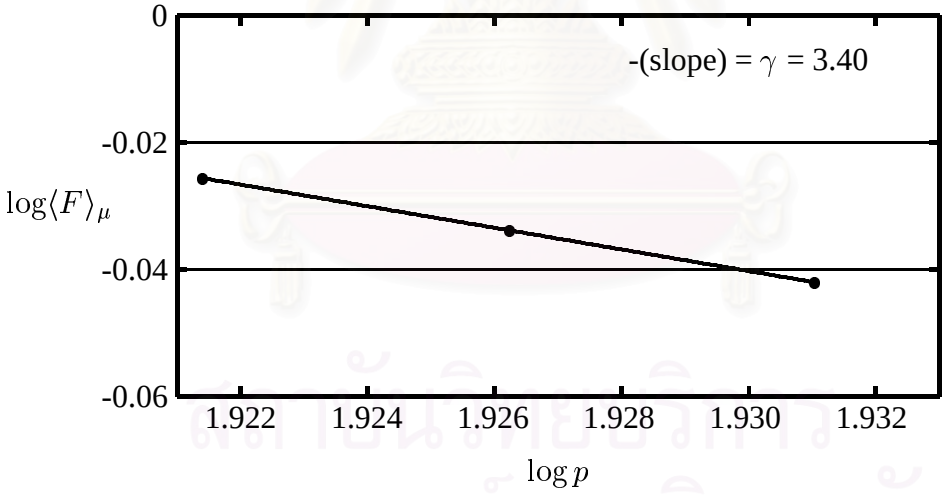

Figure 5.14: Downstream $\log\langle F\rangle_\mu$ vs. log at $v/U_{1n} = 10$, $b/\lambda_{||} = 1.0$.

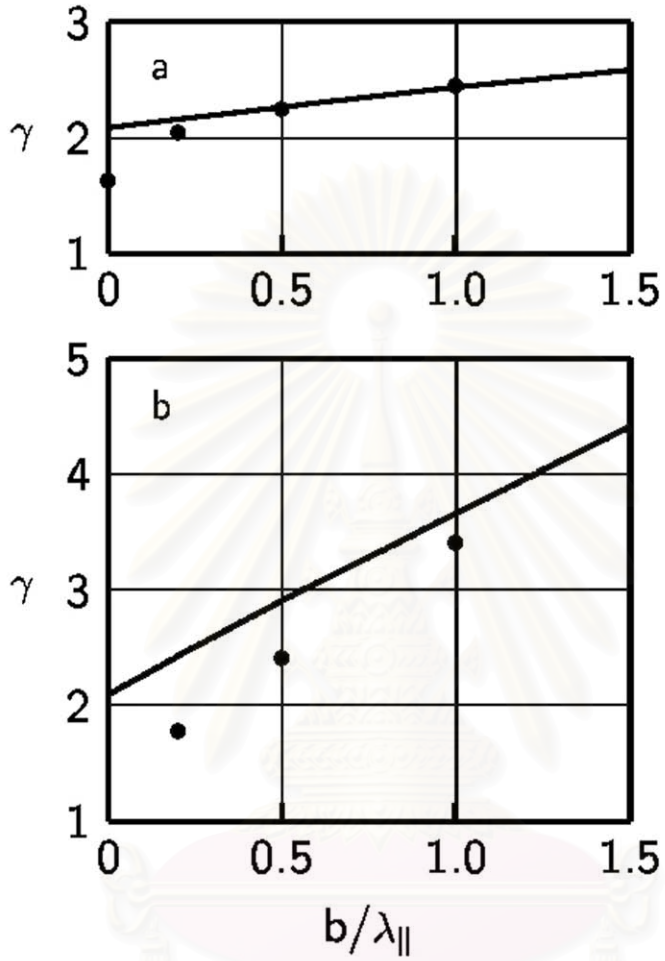

Figure 5.15: The relation between the spectral index and the compression width, $b/\lambda_{\parallel}$ for a) $v/U_{1n} = 50$ and b) $v/U_{1n} = 10$. The linear graph presents the results from the diffusion approximation, and the circles show the results from pitch-angle transport simulations.

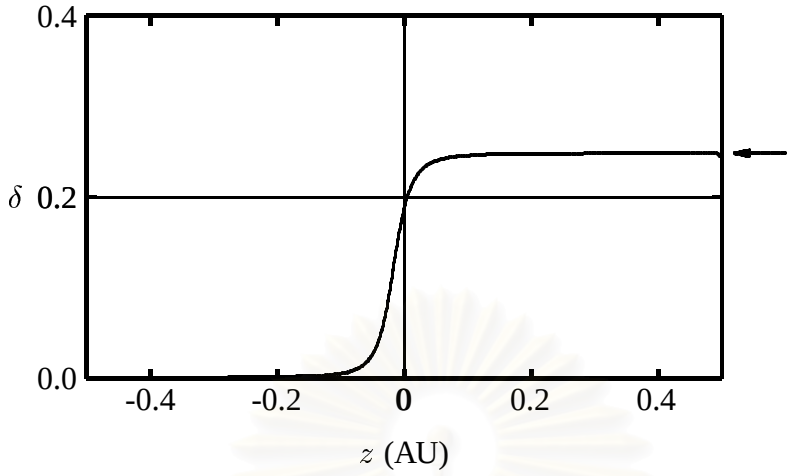

Figure 5.16: The anisotropy of the particle distribution vs. z at $v/U_{1n} = 50$, $b/\lambda_{\|} = 0.2$.

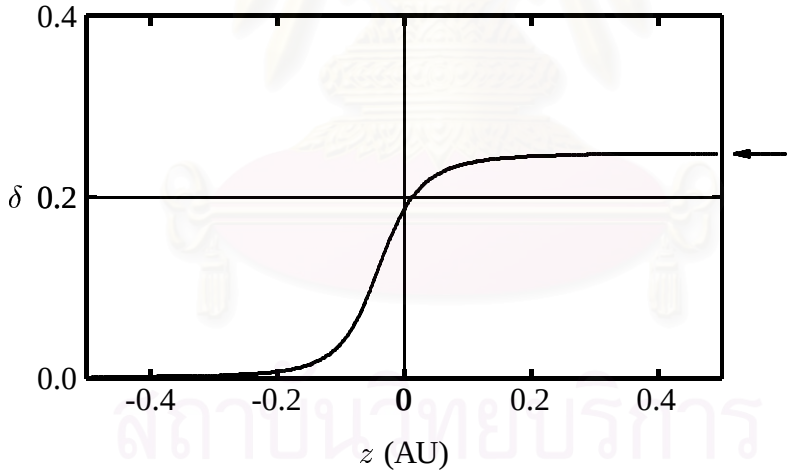

Figure 5.17: The anisotropy of the particle distribution vs. z at $v/U_{1n} = 50$, $b/\lambda_{\|} = 0.5$.

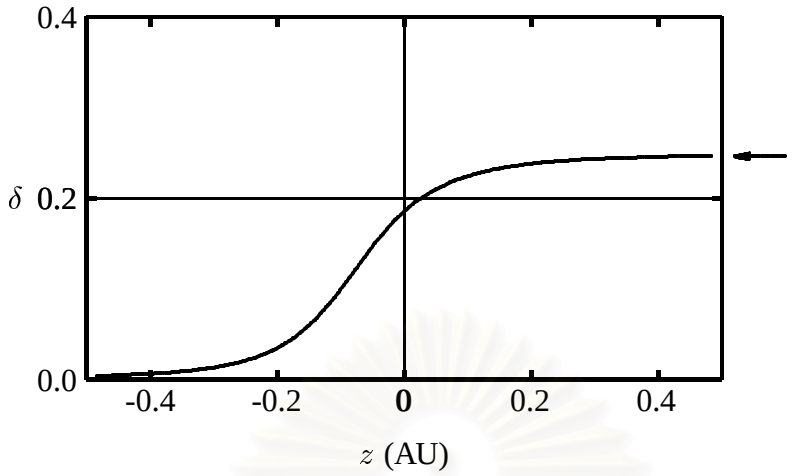

Figure 5.18: The anisotropy of the particle distribution vs. z at $v/U_{1n} = 50$, $b/\lambda_{\|} = 1.0$.

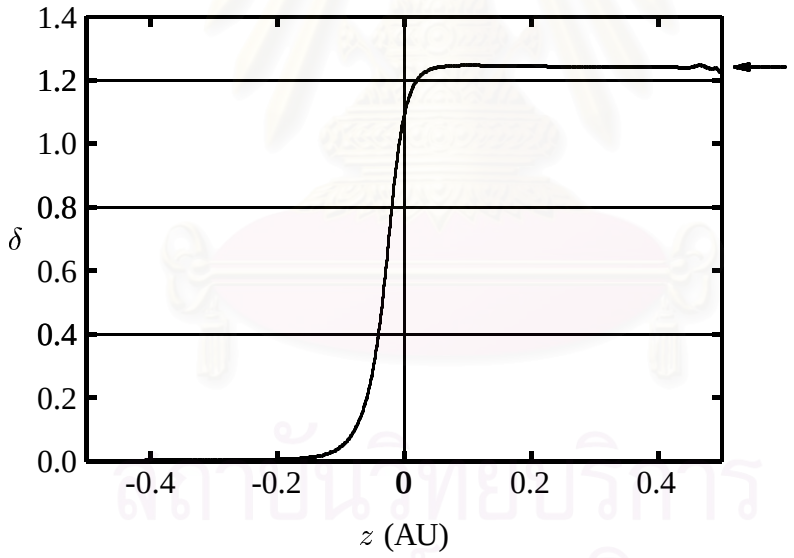

Figure 5.19: The anisotropy of the particle distribution vs. z at $v/U_{1n} = 10$, $b/\lambda_{\|} = 0.2$.

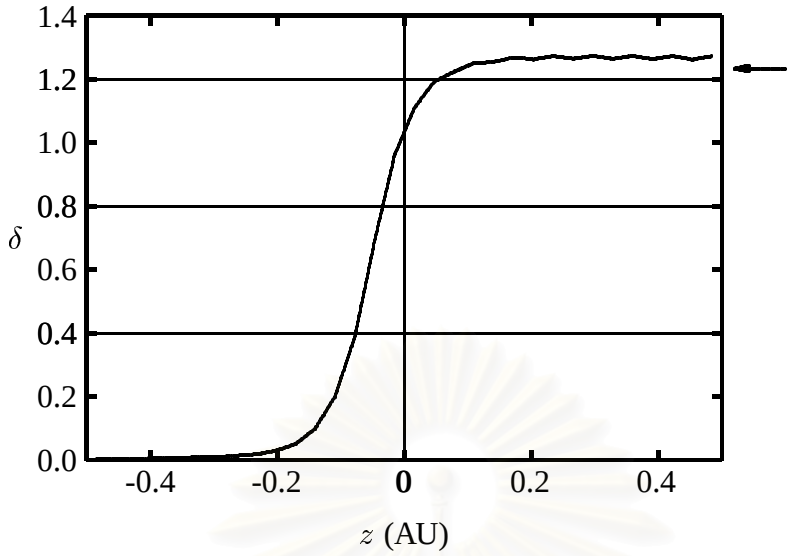

Figure 5.20: The anisotropy of the particle distribution vs. z at $v/U_{1n} = 10$, $b/\lambda_{\|} = 0.5$.

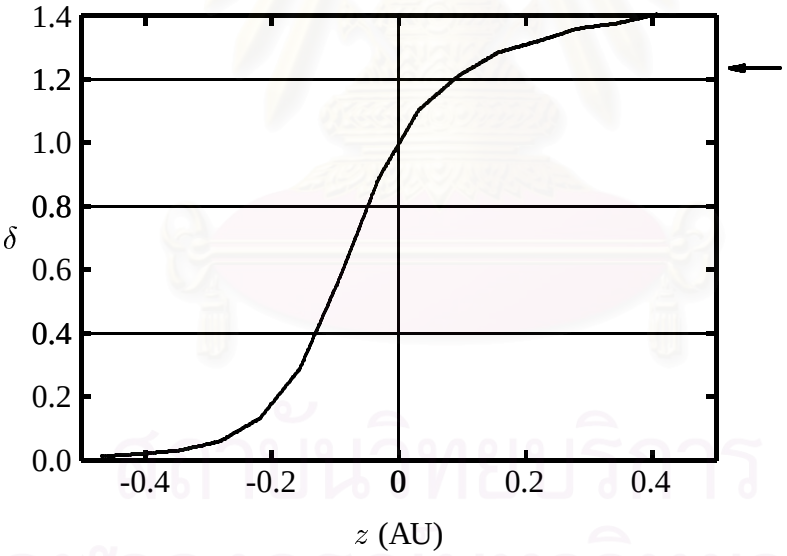

Figure 5.21: The anisotropy of the particle distribution vs. z at $v/U_{1n} = 10$, $b/\lambda_{\|} = 1.0$.

$b/\lambda_{\|}$	peak height at v/U_{1n}=50	peak height at v/U_{1n}=10
	PA	PA
shock	1.25	n/a
0.2	1.06	1.65
0.5	no peak	1.06
1.0	no peak	no peak

Table 5.1: The peak height of the particle distribution $\langle F \rangle_\mu$ vs. z at varying compression widths. PA: pitch angle transport code. The peak is not obtained in the diffusion approximation.

5.2 Discussion

The graphs of the distribution function of particles averaged over μ, $\langle F \rangle$ vs. z, as shown in Figures 5.1 - 5.4, are very different. The peak heights (normalized to the far downstream value) depend on the width of the compression region (see Table 5.1). Comparing a shock and compressions at the same momentum, the peak height is higher for a shock. The peak height then decreases with increasing compression width. When we increase the width of the compression to be equal to or larger than 0.5 (in units of $\lambda_{\|}$), a peak is not observed, except that for $v/U_{1n} = 10$, there is still a visible peak at $b/\lambda_{\|} = 0.5$. The peak in turn increases with decreasing v/U_{1n} or decreasing $b/\lambda_{\|}$. The peak height at $v/U_{1n} = 10$ for the shock is not available ("n/a") because our model cannot simulate such rapid acceleration.

Furthermore, in the upstream region we observe that the distribution function of particles is high near the compression region and decays exponentially far upstream. The rate of decay can be found by taking the logarithm of $\langle F \rangle_\mu$ far upstream and plotting $\ln\langle F \rangle_\mu$ vs. z. The slope of this graph gives the decay

$b/\lambda_{\parallel}$	decay rate at $v/U_{1n}=50$ (unit: AU^{-1})		decay rate at $v/U_{1n}=10$ (unit: AU^{-1})	
	PA	DC	PA	DC
shock	-1.03	-1.02	n/a	n/a
0.2	-1.03	-1.02	-7.60	-5.10
0.5	-1.04	-1.02	-8.11	-5.10
1.0	-1.05	-1.02	-11.66	-5.10

Table 5.2: The decay rate $\ln\langle F\rangle_\mu$ vs. z at varying compression width. PA: pitch angle transport code. DC: diffusion-convection code.

rate (see Table 5.2). We can compare this value with the analytic value from the diffusion approximation. According to §3.4, the decay rate of $\langle F\rangle_\mu$ far upstream is in the form of

$$\ln\langle F\rangle_\mu = \frac{-3U_{1n}\sec^2\theta}{v\lambda_{\parallel}}z. \tag{5.1}$$

where we express the diffusion coefficient (in z) as $D = v\lambda_{\parallel}\cos^2\theta/3$. After all values of the variables (see §4.4) are substituted into equation (5.1), we can prove that the values from the simulation at $v/U_{1n} = 50$ are similar to the values from analysis. For $v/U_{1n} = 10$, the distribution function decays more rapidly than we expected (see Table 5.2) because the distribution function is close to zero. PA and DC mean the solutions of pitch angle transport and diffusion-convection equations, respectively. We stress that the diffusion approximation only applies far from the shock or compression region. Nonetheless, it provides a useful test of the full simulation results, which are necessary for understanding the solutions near the shock or compression.

Another way to check the results from the simulations is to examine the anisotropy of the distribution function. According to the anisotropy graphs (see Figures 5.16-5.21), which are obtained in the steady-state, we see that the δ values

$b/\lambda_{\|}$	δ at v/U_{1n}=50		δ at v/U_{1n}=10	
	PA	DC	PA	DC
shock	0.24	0.24	n/a	n/a
0.2	0.24	0.24	1.23	1.23
0.5	0.24	0.24	1.25	1.23
1.0	0.25	0.24	1.40	1.23

Table 5.3: The far upstream anisotropy of the particle distribution at varying compression widths.

far downstream are nearly equal to zero and the asymptotic values far upstream are shown in Table 5.3. The values of δ at $v/U_{1n} = 50$ and $v/U_{1n} = 10$ from PA are similar to the values from DC, except at $b/\lambda_{\|} = 1.0$, where we observe that the δ from PA has a value larger than for DC because the decay of the distribution function is close to zero and the simulations become inaccurate.

In Table 5.4, the spectral index, γ, has the lowest value at a shock, which assumes that $b/\lambda_{\|} = 0$. This means that the acceleration is most efficient at a shock discontinuity. As $b/\lambda_{\|}$ increased, the value of γ also increased. The increase of γ has been reported before in the case of a parallel compression, which is the case of magnetic field lines parallel to the normal to the compression (Krülls and Achterberg 1994). In this work, we have simulated for quasi-perpendicular shocks and compressions with various momentum values and we found that the value of γ decreased with decreasing momentum. A decrease in γ means an increase in the acceleration of particles to high energy, because $F \propto p^{-\gamma}$.

Figure 5.15 shows the results of γ received from the pitch angle transport simulations (solid circles) and the diffusion-convection equation (lines). The γ value from diffusion-convection increases linearly with the compression width with

$b/\lambda_{\|}$	γ at v/U_{1n}=50		γ at v/U_{1n}=10	
	PA	DC	PA	DC
shock	1.71	2.08	n/a	2.08
0.2	2.04	2.15	1.76	2.42
0.5	2.24	2.25	2.40	2.89
1.0	2.44	2.42	3.40	3.65

Table 5.4: The spectral index of the particle distribution at varying compression width.

an approximate slope of $15\,U_{1n}/v$. At the same, at low $b/\lambda_{\|}$, where the mirroring peak is seen, the γ value from the pitch angle transport simulations is less than the diffusion-convection value. The decrease of γ at decreasing momentum has never presented before, even in work with the diffusion-convection approximation.

Note that in this work we have considered a quasi-perpendicular magnetic field ($\theta_1 = \arctan(4.0) = 75.96°$, $\theta_2 = \arctan(15.11) = 86.21°$). Further work will compare the compressions and the shock at other angles, such as quasi-parallel and intermediate cases.

Chapter 6
Conclusions

In this work we study the cosmic ray particle acceleration at a compression region by the first-order Fermi acceleration mechanism. The magnetic field configuration at the compression region is similar to that at a shock, though it is continuously curved, as shown in Figure 1.2. We use a transport equation in the form of a Fokker-Planck equation from the work of Ruffolo & Chuychai (1999) in order to describe the particle intensity in a flux tube as the function of t, z, μ, and p. We use numerical simulations in order to understand how the cosmic ray particles are accelerated.

The numerical techniques for solving the transport equation are finite difference methods, including interpolation and TVD methods. We use the operator splitting method to split our transport equation to sequentially solve for changes (motion) in each variables. In this work, we tested and debugged some codes from previous works. We control the accuracy by checking a single step of the simulation, the anisotropy of the distribution function, and the decay of the distribution function far upstream. We also compare with approximate results from the diffusion-convection equation (based on the diffusion approximation).

After numerical simulations, we obtained results for two momentum values, which expressed in terms of $v/U_{1n} = 10$ and $v/U_{1n} = 50$. We set the width of the compression regions to be $b/\lambda_{\|} = 0.2$, $b/\lambda_{\|} = 0.5$, and $b/\lambda_{\|} = 1.0$ for each momentum value. We compare results between compressions and a shock, which have different magnetic field configurations, and compare results from our transport equation and the diffusion approximation, which does not include pitch

angle transport processes.

The conclusions are:

1. Particle acceleration can occur at a continuous compression region and a shock.

2. The acceleration efficiency can be determined by the mirroring peak and the value of γ.

3. A high acceleration efficiency is found for a narrow compression width and at low momentum.

4. The mirroring peak is only found from the results of the pitch angle transport equation, for a narrow compression width.

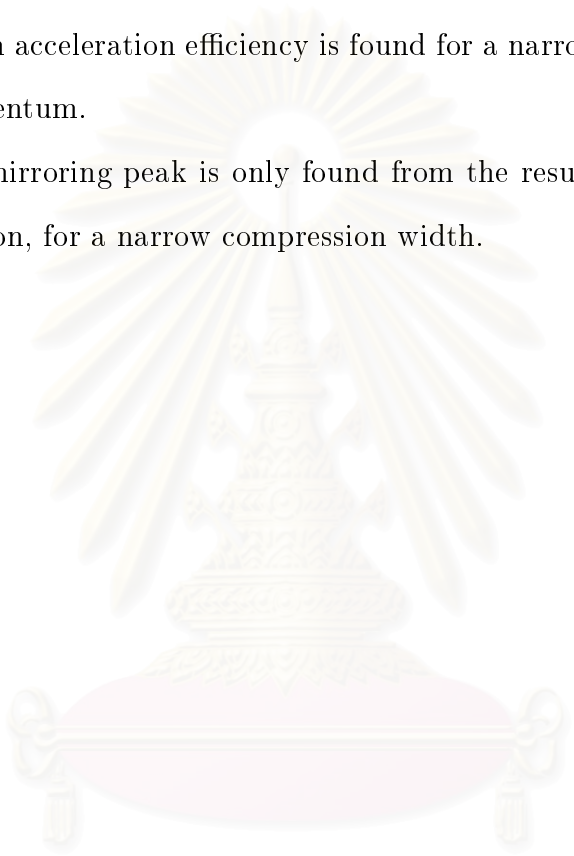

References

Bell, A. R. The acceleration of cosmic rays in shock fronts - I. Mon. Not. R. astr. Soc. **182** (1978): 147-156.

Cravens, T. E. Physics of solar system plasmas. New York: Cambridge University Press., (1997): 5.

de Hoffmann, F.,and Teller, E. Magneto-hydrodynamic shocks. Phys. Rev. **80** (1950): 692.

Earl, J. A. The effect of convection upon charged particle transport in random magnetic fields. Astrophys. J. **278** (1974): 825-840.

Fermi, E. On the origin of the cosmic radiation. Phys. Rev. **75** (1949): 1169-1174.

Fermi, E. Galactic magnetic fields and the origin of cosmic radiation. Astrophys. J. **119** (1954): 1-6.

Gieseler, U. D. J. et al. Particle acceleration at oblique shocks and discontinuities of the density profile. Astron. Astrophys. **345** (1999): 298-306.

Hatzky, R. et al. The effect of adiabatic deceleration on angular distributions of solar energetic particles. Proc. 25^{th}. Intl. Cosmic Ray Conf. **1** (1996): 245.

Harten, A. High resolution schemes for hyperbolic conservation laws. J. Comput. Phys. **49** (1983): 357.

Jokipii, J. R. Compressive-diffusive acceleration of energetic charged particles. Proc. 27^{th} Intl. Cosmic Ray Conf. **9** (2001): 3581-3584.

Krülls, W. M. et al. Computation of cosmic-ray acceleration by Itô's stochastic differential equation. Astron. Astrophys. **286** (1994): 314-327.

Krymskii, G. F. A regular mechanism for the acceleration of charged particles on the front of a shock wave. Sov. Phys. Dokl. **22 (2)** (June 1977): 327-328.

Lee, M. A.,and Ryan, J. R. Time-dependent coronal shock acceleration of energetic solar flare particles. Astrophys. J. **303** (1986): 829-824.

Mason, G. M., et al. Temporal variations of nucleonic abundances in solar flare energetic particle events, II, Evidence for large-scale shock acceleration. Astrophys. J. **280** (1984): 902-916.

Ng, C. K.,and Wong, K.-Y. Solar particle propagation under the influence of pitch-angle diffusion and collimation in the interplanetary magnetic field. Proc. 16^{th} Intl. Cosmic Ray Conf. **5** (1979): 252-257.

Nutaro, T. et al. Application of a generalized total variation diminishing algorithm to cosmic ray transport and acceleration. Computer Physics Communication **134** (2001): 209-222.

Park, B. T.,and Petrosian, V. Fokker-Planck equation of stochastic acceleration: A study of numerical methods. Astrophys. J. Suppl. **103** (1996): 255-267.

Parker, E. N. Dynamics of the interplanetary gas and magnetic fields. Astrophys. J. **128** (1958): 664-676.

Press, W. H. et al. Numerical Recipes in C. New York: Cambridge University Press, 1988.

Press, W. H. et al. Numerical Recipes in C. 2^{nd} ed. New York: Cambridge University Press, 1992.

Reames, D. V. Acceleration of energetic particles by shock waves from large solar flares. Astrophys. J. **358** (1990): L63-L67.

Roe, P. L. Some contributions to the modeling of discontinuous flows, in: B. E. Engquist et al. (Eds.), Proc. AMS/SIAM Sum. Sem. on Large-Scale Comp. in Fluid Mech., 1983, Lectures in Appl. Math., **22(2)** Amer. Math. Soc., Providence, RI, (1985).

Ruffolo, D. Effect of Adiabatic deceleration on the focused transport of solar cosmic rays. Astrophys. J. **442** (1995): 861-874.

Ruffolo, D. Charge states of solar cosmic rays and constraints on acceleration times and coronal transport. Astrophys. J. **481** (1997): L119-L122.

Ruffolo, D. Transport and acceleration of energetic charged particles near an oblique shock. Astrophys. J. **515** (1999): 787-800.

Ruffolo, D.,and Chuychai P. First-order Fermi acceleration at a continuous compression. Proc. 26^{th} Intl. Cosmic Ray Conf. **6** (1999): 552-555.

Skilling, J. Cosmic rays in the galaxy: Convection or diffusion?. Astrophys. J. **170** (1971): 265-273.

Skilling, J. Cosmic ray streaming-I. Effect of Alfvén wave on particles. Mon. Not. R. Astr. Soc. **172** (1975): 557-566.

Wax, N. Noise and stochastic processes. New York: Dover Publication, (1954): 33.

Appendices

Appendix A
C-Language Code for Treatment of Acceleration

```
/* d_peg.c -- January 21, 2001.

      Special treatment when interpolation not necessary.

      Assume that  zstep[1] = zstep_peg.

      Add condition STATICSH when finding l1, l_.

      Use interpolating between peg and p[1] in Fourth case and extrapolating
      between p[np] and p[np-1].

   d_pow.c -- January 15, 2001.

      Correcting bug: frac <-> 1-frac in interpolation formulae.
      New name clarifies boundary conditions (power laws in p).

   decel.c (v) -- April 5, 1999.

      Generalizing to treat acceleration (decelrate < 0) as well.

   decel.c (v) -- December 16, 1996.

      Version for varwind.c.

   decel.c (t) -- July 11th, 1995.

      Uses t as the independent variable instead of s.

      Note that arguments have changed!

      As a consequence of using zstep=mustep*v*timestep,
      with the same timestep for each p (instead of the same sstep=
      v*timestep), must interpolate between z values.

      Deceleration is not performed if one of the z values
      has a flux of 0 for all mu values.

   decel.c -- February 27th, 1994.

      Added more comments.  Corrected some logical errors in the
      if blocks.  Corrected a sign error in ci().  (Newton's method
      still converged, but more slowly.)

   decel -- March 13th, 1993.

      David Ruffolo and Burin Asavapibhop
      Department of Physics
      Faculty of Science
```

```
      Chulalongkorn University
      Bangkok 10330, Thailand
*/

#include   <stdio.h>
#include   <math.h>

#define   NMAX   10
#define   C      0.1202
#define   STATICSH  1
                          /* Static shock? Used to determine whether
                          nz should be an even number.          */

extern double   ***f, *fint, **peg;

void     decel(timestep,np,p,lprint,nz,zstep,nmu,vsw,printextra)
double   timestep, *p, *zstep, vsw; int      np, nmu, printextra;
long     lprint, *nz; {
   FILE     *fp_g;
   double   expon, frac, lnp_, lnp0, lnp1, *lower, mu, mustep, pi, *upper, z;
   int      allzero, u, w, rnp;
   long     l_, l0, l1;

   static double p0;
   static int    first=1;
   static long   rnz;

   double   decelrate();

   void     nrerror();

   if (printextra) printf("Entering decel()...\n");

   if (first) {
      if ((fp_g = fopen("peg.dat","r")) == NULL)
         nrerror("stream: peg.dat not found");
      fscanf(fp_g,"%d\n",&rnp);
      if (rnp != 1) nrerror("stream: rnp != 1");
      fscanf(fp_g,"%lf\n",&p0);
      fscanf(fp_g,"%ld\n",&rnz);

      first=0;
   }

   mustep  = 2.0;
   mustep /= nmu;
   lower = upper = fint;
   for (u=1;u<=nmu;u++) upper[u] = 0.0;

      /* Away from the p-boundaries:

         pf is constant along straight lines (characteristics) in a plot
         of ln(p) vs. t.  Therefore, we find the point in the ln(p) vs. t
         plane where the constant-t line intersects the characteristic
         passing through (t+delta t,p).  f is interpolated between
         p and the next higher p-grid point along the constant-t line
         to find pf at the intersection point, which is then pf at
         the next time step.

         A slight complication when using t in place of s: f at the
         desired z at the next higher p is found by interpolation
```

```
      between adjacent z values, except when f(mu) is identically
      0 at one of those values.

      0  -> quantities at the original grid point.
      _  -> the next lower p-grid point.
      1  -> the next higher p-grid point.
      pi -> the characteristic-intersection (ci) point.
   */

for (w=1;w<=np;w++) {
   if (w==1) lnp_ = log(p0);
   if (w>1) lnp_ = log(p[w-1]);
   lnp0 = log(p[w]);
   if (w<np) lnp1 = log(p[w+1]);
   for (l0=1;l0<=nz[w];l0++) {
      if (STATICSH) {
         z = zstep[w]*(l0-nz[w]/2.0-0.5);
      } else {
         z = zstep[w]*(l0-0.5);
      }

         /* If f[w][l0][u] < 0, bomb out. */

      if (f[w][l0][u] < 0) {
         printf("w = %d, l = %ld, u = %d\n",w,l0,u);
         nrerror("decel: f < 0");
      }

         /* First case: decelerating, and away from boundary. */

      if (decelrate(z,mu,vsw)>0 && w < np) {

        /* Find upper[u], the z-interpolated value of f
       at (t,z,p1).
        */
         if (STATICSH){
        l1 = z/zstep[w+1] + nz[w+1]/2.0 + 0.5;
        frac = z/zstep[w+1] + nz[w+1]/2.0 + 0.5 - (double)l1;
      }else{
         l1 = z/zstep[w+1] + 0.5;
         frac = z/zstep[w+1] + 0.5 - (double)l1;
          }

            /* Special case: if frac is very close to 0 or 1, no
               need to interpolate. */

         if (fabs(frac)<1e-6 || fabs(frac-1.0)<1e-6) {
            if (fabs(frac-1.0)<1e-6) l1++;
            if (l1 < 1 || l1 > nz[w+1]) {
           for (u=1;u<=nmu;u++) upper[u] = 0.0;
            } else {
       for (u=1;u<=nmu;u++) upper[u] = f[w+1][l1][u];
            }
         } else {

          if (l1 < 1 || l1+1 > nz[w+1]) {
        for (u=1;u<=nmu;u++) upper[u] = 0.0;
         } else {
        for (allzero=1,u=1;allzero && u<=nmu;u++)
           allzero = f[w+1][l1][u] == 0.0;
```

```
  if (!allzero)
     for (allzero=1,u=1;allzero && u<=nmu;u++)
    allzero = f[w+1][l1+1][u] == 0.0;
  if (allzero) {
     for (u=1;u<=nmu;u++) upper[u] = 0.0;
  } else {
     for (u=1;u<=nmu;u++)
      upper[u] = (1.0-frac)*f[w+1][l1][u] + frac*f[w+1][l1+1][u];
  }
   }
    }

   /* If f0 or f1 is 0, do not proceed.  If one of them
  is non-zero, warn the user.
   */

for (u=1;u<=nmu;u++) {
   if (f[w][l0][u]*upper[u] == 0.0) {
  if (printextra && l0%lprint==1 && w==1 && f[w][l0][u]!=0.0) {
     printf("\nNote: f[%d][%d][%d] = %le, upper[%d] = 0",
    w,l0,u,f[w][l0][u],u);
  } else if (printextra && l0%lprint==1 && w==1 &&
    upper[u] != 0.0) {
     printf("\nNote: f[%d][%d][%d] = 0, upper[%d] = %le",
    w,l0,u,u,upper[u]);
  }
   } else {
  mu = -1.0 + (u-0.5)*mustep;

     /* dp/dt = -p / deceltime = -p*decelrate */

  pi = p[w] * exp(timestep*decelrate(z,mu,vsw));

     /* Power-law interpolation.  expon is the slope
    on a log-log plot from (p0,f0) to (p1,f1).
     */

  expon = (log(upper[u])-log(f[w][l0][u])) / (lnp1-lnp0);

  f[w][l0][u] *= pow(pi/p[w],1.0+expon);
   }
}

    /* Second case: change from d_pow.c by extrapolating between
       p[np] and p[np-1] for finding pF at the next time step and
       it's added in the 3rd case.

       Third case: accelerating, and away from boundary.

 } else if (decelrate(z,mu,vsw)<0 && w > 1) {

   /* Find lower[u], the z-interpolated value of f
  at (t,z,p[w-1]).
   */
    if (STATICSH){
   l_ = z/zstep[w-1] + nz[w-1]/2.0 + 0.5;
   frac = z/zstep[w-1] + nz[w-1]/2.0 + 0.5 - (double)l_;
    }else{
   l_ = z/zstep[w-1] + 0.5;
   frac = z/zstep[w-1] + 0.5 - (double)l_;
    }
```

```
        /* Special case: if frac is very close to 0 or 1, no
           need to interpolate. */

     if (fabs(frac)<1e-6 || fabs(frac-1.0)<1e-6) {
        if (fabs(frac-1.0)<1e-6) l_++;
        if (l_ < 1 || l_ > nz[w-1]) {
       for (u=1;u<=nmu;u++) lower[u] = 0.0;
        } else {
  for (u=1;u<=nmu;u++) lower[u] = f[w-1][l_][u];
        }
     } else {
    if (l_ < 1 || l_+1 > nz[w-1]) {
  for (u=1;u<=nmu;u++) lower[u] = 0.0;
    } else {
  for (allzero=1,u=1;allzero && u<=nmu;u++)
     allzero = f[w-1][l_][u] == 0.0;
  if (!allzero)
     for (allzero=1,u=1;allzero && u<=nmu;u++)
    allzero = f[w-1][l_+1][u] == 0.0;
  if (allzero) {
     for (u=1;u<=nmu;u++) lower[u] = 0.0;
  } else {
     for (u=1;u<=nmu;u++)
      lower[u] = (1.0-frac)*f[w-1][l_][u] + frac*f[w-1][l_+1][u];
  }
    }
}

   /* If f0 or f_ is 0, do not proceed.  If one of them
  is non-zero, warn the user.
   */

for (u=1;u<=nmu;u++) {
   if (f[w][l0][u]*lower[u] == 0.0) {
  if (printextra && l0%lprint==1 && w==1 && f[w][l0][u]!=0.0) {
     printf("\nNote: f[%d][%d][%d] = %le, upper[%d] = 0",
    w,l0,u,f[w][l0][u],u);
  } else if (printextra && l0%lprint==1 && w==1 &&
    lower[u] != 0.0) {
     printf("\nNote: f[%d][%d][%d] = 0, upper[%d] = %le",
    w,l0,u,u,lower[u]);
  }
   } else {
  mu = -1.0 + (u-0.5)*mustep;

     /* dp/dt = -p / deceltime = -p*decelrate */

  pi = p[w] * exp(timestep*decelrate(z,mu,vsw));

     /* Power-law interpolation.  expon is the slope
    on a log-log plot from (p0,f0) to (p1,f1).
     */

  expon = (log(lower[u])-log(f[w][l0][u])) / (lnp_-lnp0);

  f[w][l0][u] *= pow(pi/p[w],1.0+expon);
   }
}

   /* Fourth case: treatment for the lowest p-grid point. */

 } else if (decelrate(z,mu,vsw)<0 && w == 1) {
```

```
   /* Find lower[u], the z-interpolated value of f
  at (t,z,p_peg).
   */


    if (STATICSH){
   l_ = z/zstep[1] + nz[1]/2.0 + 0.5;
   frac = z/zstep[1] + nz[1]/2.0 + 0.5 - (double)l_;
    }else{
   l_ = z/zstep[1] + 0.5;
   frac = z/zstep[1] + 0.5 - (double)l_;
    }
       /* Special case: if frac is very close to 0 or 1, no
          need to interpolate. */

    if (fabs(frac)<1e-6 || fabs(frac-1.0)<1e-6) {
       if (fabs(frac-1.0)<1e-6) l_++;
       if (l_ < 1 || l_ > nz[1]) {
      for (u=1;u<=nmu;u++) lower[u] = 0.0;
       } else {
  for (u=1;u<=nmu;u++) lower[u] = peg[l_][u];
       }
    } else {
   if (l_ < 1 || l_+1 > nz[w]) {
  for (u=1;u<=nmu;u++) lower[u] = 0.0;
   } else {
  for (allzero=1,u=1;allzero && u<=nmu;u++)
     allzero = peg[l_][u] == 0.0;
  if (!allzero)
     for (allzero=1,u=1;allzero && u<=nmu;u++)
    allzero = peg[l_+1][u] == 0.0;
  if (allzero) {
     for (u=1;u<=nmu;u++) lower[u] = 0.0;
  } else {
     for (u=1;u<=nmu;u++)
      lower[u] = (1.0-frac)*peg[l_][u] + frac*peg[l_+1][u];
  }
   }
}

   /* If f0 or f_ is 0, do not proceed.  If one of them
  is non-zero, warn the user.
   */

for (u=1;u<=nmu;u++) {
   if (f[w][l0][u]*lower[u] == 0.0) {
  if (printextra && l0%lprint==1 && w==1 && f[w][l0][u]!=0.0) {
     printf("\nNote: f[%d][%d][%d] = %le, upper[%d] = 0",
    w,l0,u,f[w][l0][u],u);
  } else if (printextra && l0%lprint==1 && w==1 &&
     lower[u] != 0.0) {
      printf("\nNote: f[%d][%d][%d] = 0, upper[%d] = %le",
    w,l0,u,u,lower[u]);
  }
   } else {
  mu = -1.0 + (u-0.5)*mustep;

     /* dp/dt = -p / deceltime = -p*decelrate */

  pi = p[w] * exp(timestep*decelrate(z,mu,vsw));
```

```
            /* Power-law interpolation.  expon is the slope
           on a log-log plot from (p0,f0) to (p1,f1).
            */

          expon = (log(lower[u])-log(f[1][l0][u])) / (lnp_-lnp0);

          f[1][l0][u] *= pow(pi/p[w],1.0+expon);
           }
        }
         }
      }
   }

   if (printextra) printf("...and leaving decel().\n");
}
```

Appendix B

Program for Testing: Evaluation of $\partial F/\partial t$ for $F \equiv 1$

```
/* Calculate Each components of (1/F)dF/dt (which are: Streaming,
Scattering & Focusing, and Deceleration by varying z from
-16*zstep to 16*zstep (length=5, zstep=0.0062525)and mu from
1*mustep to 15*mustep (mustep = 2.0/15). Lambda =1, Gamma=1.65,
PB=0.2. This program is actually used for checking (1/F)(dF/dt)
which parallels to the code varwind.diag.c which we have run it
for one timestep(2.86325)in 0705C.*/

#include<stdio.h>
#include<math.h>

#define   C     0.1202
#define   PI (4.0*atan(1.0))
#define THETA1 atan(4.0)
#define THETA2 atan(15.11)
#define PB 0.2
#define S -1

void main(void) {
   FILE     *fp_out;
   double   dUzdz(), divl(), Udotl(), lldUdz(), divU();
   double   lz(), Uz(), dydz(), ddydz();
   double   z, mu, zstep, mustep, length;
   int      u, l, nmu;
   double   vsw,v,lambda, gamma;
   double   str, decel, scf, scf1, scf2, scf3, scf4, scf5, scf6, scf7, scf8;

   vsw=0.001816*C;
   v=0.001816*10*C;
   nmu=15;
   zstep=0.00625;
   lambda=1.0;
   gamma=1.65;

   mustep=2.0/(double)nmu;

   fp_out=fopen("stream.dat","w");
   for (u=1;u<=nmu;u++){
       mu=-1.0+(u-0.5)*mustep;
       for (l=-15;l<=16;l++){
      z = (l-0.5)*zstep;
      str= -dUzdz(z,vsw)-mu*v*divl(z)+(mu*mu*v*v/(C*C))*
           (Udotl(z,vsw)*divl(z)+lldUdz(z,vsw)+Udotl(z,vsw)
           *divl(z));
      fprintf(fp_out,"%.8lf    ",str*2.86325);
       }
       fprintf(fp_out,"\n");
    }
```

```
    fclose(fp_out);


   fp_out=fopen("scattfo.dat","w");
       for (u=1;u<=nmu;u++){
       mu=-1.0+(u-0.5)*mustep;
           for (l=-15;l<=16;l++){
              z=(l-0.5)*zstep;
              scf=mu*(v*divl(z)+mu*divU(z,vsw)-3*mu*lldUdz(z,vsw)-
                  (mu*v*v/(C*C))*Udotl(z,vsw)*divl(z))
                  +(v/lambda)*mu*v*Udotl(z,vsw)/(C*C)
                  +(-(1-(mu*mu))/2)*(divU(z,vsw)-3*lldUdz(z,vsw)
                  -(v*v/(C*C))*Udotl(z,vsw)*divl(z));
              fprintf(fp_out,"%.8lf    ",scf*2.86325*0.5);

           }
           fprintf(fp_out,"\n");
       }
    fclose(fp_out);

   fp_out=fopen("scf.dat","w");
       for (u=1;u<=nmu;u++){
       mu=-1.0+(u-0.5)*mustep;
           for (l=-15;l<=16;l++){
              z=(l-0.5)*zstep;
              scf1=mu*v*divl(z);
              scf2=mu*mu*divU(z,vsw);
              scf3=mu*(-3*mu*lldUdz(z,vsw));
              scf4=mu*(-mu*v*v/(C*C))*Udotl(z,vsw)*divl(z);
              scf5=(v/lambda)*mu*v*Udotl(z,vsw)/(C*C);
              scf6=(-(1-(mu*mu))/2)*divU(z,vsw);
              scf7=(-(1-(mu*mu))/2)*(-3*lldUdz(z,vsw));
              scf8=(-(1-(mu*mu))/2)*(-v*v/(C*C))*Udotl(z,vsw)*divl(z);
              if(u==1 && l==0){
                 fprintf(fp_out,"%.8lf\n%.8lf\n%.8lf\n%.8lf\n%.8lf\n
                                 %.8lf\n%.8lf\n%.8lf\n"
                                ,scf1,scf2,scf3,scf4,scf5,scf6,scf7,scf8);
              }
           }
       }
    fclose(fp_out);

   fp_out=fopen("decel.dat","w");
       for (u=1;u<=nmu;u++){
       mu=-1.0+(u-0.5)*mustep;
           for (l=-15;l<=16;l++){
               z=(l-0.5)*zstep;
               decel=(gamma-1)*(((1-mu*mu)/2)*(lldUdz(z,vsw)-divU(z,vsw))
                     -mu*mu*lldUdz(z,vsw));
               fprintf(fp_out,"%.8lf    ",decel*2.86325);
          }
          fprintf(fp_out,"\n");
       }
    fclose(fp_out);
 }

double   dydz(z) double   z; {
   double terma,termb,termc,th,th_h,out;
   double sec2th_h,tan2th_h,dbdz,dcdz;

   th_h = fabs(THETA1-THETA2) / 2;
```

```
   if (THETA2 > THETA1)   th = -(THETA1+th_h);
   if (THETA1 > THETA2)   th = -(THETA2+th_h);
   tan2th_h = tan(th_h) * tan(th_h);
   sec2th_h = 1+tan2th_h;
   terma    = 1 - sec2th_h*sin(th)*sin(th);
   termb    = -z*sec2th_h*sin(2*th) - 2*S*PB*tan(th_h)*cos(th);
   termc    = z*z*sec2th_h*sin(th)*sin(th)
              + 2*z*S*PB*tan(th_h)*sin(th)- z*z*tan2th_h;
   dbdz     = -sec2th_h*sin(2*th);
   dcdz     = 2*z*sec2th_h*sin(th)*sin(th)
              + 2*S*PB*tan(th_h)*sin(th)- 2*z*tan2th_h;
   out      =  (0.5/terma) * (-dbdz - S*(termb*dbdz-2*terma*dcdz)
        /sqrt(termb*termb-4*terma*termc));
   return(out);
}

/*    ddydz
      THIS ROUTINE CALCULATES SECOND DERIVATIVE OF HYPER. FUNC.
*/

double   ddydz(z) double   z; {
   double terma,termb,termc,th,th_h,out;
   double sec2th_h,tan2th_h,dbdz,dcdz,ddcdz,first,second;

   th_h = fabs(THETA1-THETA2) / 2;
   if (THETA2 > THETA1)   th = -(THETA1+th_h);
   if (THETA1 > THETA2)   th = -(THETA2+th_h);
   tan2th_h = tan(th_h) * tan(th_h);
   sec2th_h = 1+tan2th_h;
   terma    = 1 - sec2th_h*sin(th)*sin(th);
   termb    = -z*sec2th_h*sin(2*th) - 2*S*PB*tan(th_h)*cos(th);
   termc    = z*z*sec2th_h*sin(th)*sin(th) + 2*z*S*PB*tan(th_h)*sin(th)
        - z*z*tan2th_h;
   dbdz     = -sec2th_h*sin(2*th);
   dcdz     = 2*z*sec2th_h*sin(th)*sin(th)
              + 2*S*PB*tan(th_h)*sin(th)- 2*z*tan2th_h;
   ddcdz    = 2*sec2th_h*sin(th)*sin(th)  - 2*tan2th_h;
   first    = (dbdz*dbdz-2*terma*ddcdz) / sqrt(termb*termb-4*terma*termc);
   second   = (termb*dbdz-2*terma*dcdz)*(termb*dbdz-2*terma*dcdz)
        / ((termb*termb-4*terma*termc)
           *sqrt(termb*termb-4*terma*termc));
   out      =  (0.5/terma) * (-S*(first-second));

   return(out);
}

/*    Uz
      THIS ROUTINE CALCULATES SOLAR WIND SPEED
      ALONG z COMPONENT.
*/

double   Uz(z,vsw) double   z,vsw;

{
   double dydz();


   return(vsw*tan(THETA1)/dydz(z));
}


/*    lz
```

```
      THIS ROUTINE CALCULATES THE z-COMPONENT OF THE UNIT VECTOR l
      (IN THE DIRECTION TO B).
*/


double   lz(z) double   z; {
   double dydz();


   return(1 / sqrt(dydz(z)*dydz(z)+1));
}

/*    Udotl
      THIS ROUTINE CALCULATES THE DOT PRODUCT BETWEEN U AND l.
*/


double   Udotl(z,vsw) double   z,vsw; {
   double Uz(),lz();

   return(Uz(z,vsw)*lz(z));
}

/*    dUzdz
      THIS ROUTINE CALCULATES dUz/dz.
*/


double   dUzdz(z,vsw) double   z,vsw; {
   double Uz(),dydz(),ddydz();

   return(-Uz(z,vsw)*ddydz(z)/dydz(z));
}

/*    lldUdz
      THIS ROUTINE CALCULATES lzlzdU/dz.
*/

double   lldUdz(z,vsw) double   z,vsw; {
   double lz(),dUzdz();

   return(lz(z)*lz(z)*dUzdz(z,vsw));
}

/*    divU
      THIS ROUTINE CALCULATES THE DIVERGENCE OF VECTOR U.
*/

double   divU(z,vsw) double   z,vsw; {
   double dUzdz();

   return(dUzdz(z,vsw));
} /*    dUzdz
      THIS ROUTINE CALCULATES THE DIVERGENCE OF UNIT VECTOR l.
*/


double   divl(z) double   z; {
   double lz(),dydz(),ddydz();

   return(-dydz(z)*ddydz(z)*lz(z)*lz(z)*lz(z));
}
```

Vitae

Kamonporn Klappong

1976 Born: Sep., 29th 1976 in Nakhon Si Thammarat, THAILAND.
Farther: Kowit Klappong.
Mother: Ugsorn Klappong.

1995-1998 Bachelor of Science (Physics),
Mahidol University, Bangkok, THAILAND.

National and International Conference Presentations

2001 Klappong, K.; Leerungnavarat, K.; Chuychai, P.; Ruffolo, D. Particle Acceleration and pitch angle transport near a thin shock, a compression region. 27th Congress on Science and Technology of Thailand (Songkla) (October 2001): 372.

2001 Klappong, K.; Leerungnavarat, K. (presenter); Chuychai, P.; Ruffolo, D. Particle acceleration and pitch angle transport near a thin shock, a compression region, and a structured shock. Proc. 27th Intl. Cosmic Ray Conf. (August 2001): 3461.

2001 Klappong, K.; Leerungnavarat, K.; Chuychai, P.; Hirunsirisawat, E.; Ruffolo, D. Comparison between particle acceleration at a continuous compression and at a shock. Proc. 5th Ann. Symp. Computational Sci. and Eng. (Thailand) (June 2001): 119.